

# Mars Odyssey measurements of galactic cosmic rays and solar particles in Mars orbit, 2002–2008

C. Zeitlin,<sup>1,2</sup> W. Boynton,<sup>3</sup> I. Mitrofanov,<sup>4</sup> D. Hassler,<sup>1</sup> W. Atwell,<sup>5</sup> T. F. Cleghorn,<sup>6</sup> F. A. Cucinotta,<sup>6</sup> M. Dayeh,<sup>7</sup> M. Desai,<sup>7</sup> S. B. Guedersloh,<sup>8</sup> K. Kozarev,<sup>9</sup> K. T. Lee,<sup>6</sup> L. Pinsky,<sup>10</sup> P. Saganti,<sup>11</sup> N. A. Schwadron,<sup>9</sup> and R. Turner<sup>12</sup>

Received 22 December 2009; revised 30 July 2010; accepted 4 August 2010; published 11 November 2010.

[1] The instrument payload aboard the 2001 Mars Odyssey orbiter includes several instruments that are sensitive to energetic charged particles from the galactic cosmic rays (GCR) and solar particle events (SPE). The Martian Radiation Environment Experiment (MARIE) was a dedicated energetic charged particle spectrometer, but it ceased functioning during the large solar storm of October/November 2003. Data from two other Odyssey instruments are used here: the Gamma Ray Spectrometer and the scintillator component of the High Energy Neutron Detector. Though not primarily designed to measure energetic charged particles, both systems are sensitive to them, and several years of data are available from both. Using the MARIE data for calibration of the other systems, count rates can be normalized (with significant uncertainties) to absolute fluxes of both GCR and solar energetic particles (SEP). The data, which cover the time span from early 2002 through the end of 2007, clearly show the solar cycle-dependent modulation of the GCR starting in 2004. Many SPEs were recorded as well and are cataloged here. Threshold energies were relatively high, ranging from 16 MeV in the most sensitive channel to 42 MeV. These thresholds are not optimal for detailed studies of SEPs, but this is the range of interest for calculations of dose and dose equivalent, pertinent to human flight, and covering that range was the original motivation for MARIE. The data are available on request and are potentially of use for the Earth-Moon-Mars Radiation Environment Module collaboration and other heliospheric modeling projects.

**Citation:** Zeitlin, C., et al. (2010), Mars Odyssey measurements of galactic cosmic rays and solar particles in Mars orbit, 2002–2008, *Space Weather*, 8, S00E06, doi:10.1029/2009SW000563.

## 1. Introduction

[2] Humans on long-duration space missions to the Moon and Mars will receive radiation doses from ener-

getic particles including heavy ions, with possible detrimental health effects such as cataract and cancer induction [Committee on the Evaluation of Radiation Shielding for Space Exploration, National Research Council, 2008], damage to the central nervous system [Vazquez, 1998], and acute effects which may be caused by an intense solar particle event (SPE) if one were to occur with astronauts in an unshielded or minimally shielded environment [Townsend et al., 1992]. As a precursor to human travel in deep space, the 2001 Mars Odyssey instrument payload [Saunders et al., 2004] included the Martian Radiation Environment Experiment (MARIE) [Badhwar, 2004; Zeitlin et al., 2004], intended to make the first detailed measurements of energetic charged particles at Mars. For purposes of radiation dosimetry as it pertains to astronaut health, “energetic” protons and heavy ions can be considered those with kinetic energies above about 20 MeV/nuc; at these energies, protons have ranges sufficient to penetrate many parts of existing spacesuits [Moyers et al., 2006] and deposit dose to the skin and deeper locations in the body.

<sup>1</sup>Southwest Research Institute, Boulder, Colorado, USA.

<sup>2</sup>Lawrence Berkeley National Laboratory, Berkeley, California, USA.

<sup>3</sup>Lunar and Planetary Laboratory, University of Arizona, Tucson, Arizona, USA.

<sup>4</sup>Space Research Institute, Moscow, Russia.

<sup>5</sup>Boeing Company, Houston, Texas, USA.

<sup>6</sup>NASA Johnson Space Center, Houston, Texas, USA.

<sup>7</sup>Southwest Research Institute, San Antonio, Texas, USA.

<sup>8</sup>Department of Nuclear Engineering, Texas A&M University, College Station, Texas, USA.

<sup>9</sup>Department of Astronomy, Boston University, Boston, Massachusetts, USA.

<sup>10</sup>Physics Department, University of Houston, Houston, Texas, USA.

<sup>11</sup>Department of Physics, Prairie View A&M University, Prairie View, Texas, USA.

<sup>12</sup>Analytic Services Inc., Arlington, Virginia, USA.

[3] The principal sources of energetic charged particle radiation in deep space are the galactic cosmic rays (GCR) and solar particle events. The GCR flux is continuous and variable, reaching maximum intensity near solar minimum, and vice versa. The GCR flux consists [Badhwar and O'Neill, 1992] mainly of protons (85%–90%) and helium (about 11%), with about 1% electrons and another 1% heavy ions. The latter are sometimes referred to as "HZE" particles, for high charge ( $Z$ ) and energy ( $E$ ). These are defined as the bare nuclei of lithium ( $Z = 3$ ) and all heavier elements, fully stripped of their electrons. Though they comprise a small part of the flux, GCR heavy ions contribute a large share of the dose and dose equivalent (the quantity used to estimate cancer risk) in unshielded or lightly shielded deep space environments. SPE can be hazardous to astronauts, particularly outside the geomagnetosphere and when shielding is minimal (e.g., on EVA, the lunar surface, etc.). Some events contain substantial fluxes of high-energy protons; these are of particular concern, as are those rare events in which substantial fluxes of HZE ions are accelerated [Tylka and Dietrich, 1999]. Spectral "hardness" is often characterized by fitting the differential flux,  $dJ/dE$ , with a power law, i.e.,  $dJ/dE \propto E^{-\gamma}$ . So-called "hard events" that may contribute significant dose behind shielding are characterized by values of  $\gamma$  above 3.

### 1.1. The 2001 Mars Odyssey Overview

[4] The Odyssey spacecraft, scientific payload, and mission goals are described in detail in the mission overview [Saunders et al., 2004]. Although the Odyssey payload nominally consists of three instruments, THEMIS, GRS, and MARIE, the GRS is actually an instrument suite consisting of three subsystems, the gamma ray detector built by the University of Arizona, the Neutron Spectrometer (NS) from Los Alamos National Laboratory, and the High Energy Neutron Detector (HEND) from the Russian Space Science Institute [Boynton et al., 2004]. The HEND itself consists of five sensors, covering various ranges of neutron energies. Thus, Odyssey actually contains nine sensors, eight of which have either direct or indirect sensitivity to energetic charged particles.

[5] Odyssey was launched in April 2001 and arrived at Mars in October 2001. Science operations began in February 2002, after the orbit was stabilized. The orbit is circumpolar at an altitude that varies from about 390 km at periapsis, approximately above the South Pole, to about 450 km at apoapsis, with a period just under 2 h. (The period varies slightly but is close to 118.5 min.) The local mean solar time has changed throughout the mission, but for the time period described here was mostly stable at 0500 LMST/1700 LMST. In 2008, a maneuver was initiated to move the orbit to 0345/1545 LMST to improve the signal to noise in the thermal imaging system. At the earlier orbit time, the GRS cannot be operated due to thermal issues.

[6] Odyssey's primary science goal, successfully achieved early in the mission [Boynton et al., 2002], was to search

for evidence of water on Mars. The search for buried water makes use of nuclear physics techniques based on the detection of gamma rays and neutrons of various energies [Lingenfelter et al., 1961], which are produced when GCR penetrate the Martian atmosphere and some depth into the soil, and undergo nuclear interactions. The Gamma Ray Spectrometer suite, including HEND and the Neutron Spectrometer (NS), are designed to measure secondary particles produced by the interactions of primary energetic GCR and solar particles; the instruments therefore indirectly measure the local energetic particle environment.

### 1.2. Objectives and Organization

[7] Following the failure of MARIE in late October 2003, the GRS and HEND provide a record of the time-varying charged particle environment in Mars orbit, but information about the composition is not available. In this work, we have selected the channels with the greatest sensitivity to energetic charged particles, and we use the period during which MARIE was functioning to make estimates of the relative calibrations of the instruments for purposes of understanding the incident flux, dose, and dose equivalent over several years of the mission.

[8] With the clarity of hindsight, we can say that MARIE was not adequately calibrated prior to flight. It was also quite limited in dynamic range and rate capability, as explained in detail below. GRS and HEND were designed for other purposes and were also not calibrated with charged particle beams prior to flight. Our understanding of the instrument responses, including the crucially important MARIE trigger thresholds, must therefore come from analysis of the flight data itself. The MARIE trigger thresholds are of particular significance; they cannot be studied by simulation, and attempts to study the thresholds using the similar (but not identical) flight spare yielded an unfortunately muddled picture (see Appendix A for details).

[9] Our purpose in this paper is twofold: first, to understand the responses of the three instruments used, and, second, to apply this understanding to the data obtained by GRS and HEND after MARIE failed. The resulting data cover a significant portion of Solar Cycle 23 from the unique vantage point of Mars orbit. We believe the SPE observations are of particular interest. Below, we show a comparison between the Earth-Moon-Mars Radiation Environment Module (EMMREM) model [Schwadron et al., 2010] and our data. Since 25 SPEs of varying intensity are reported here, many more comparisons of this type are possible, and all data presented here are freely available from the corresponding author.

[10] We present this study in three main parts. First, we describe the instruments and our general approach to normalization of count rate data. Second, we focus on the period of successful MARIE operation, from March 2002 through October 2003, with the primary goal of using the (comparatively) well-understood MARIE data to characterize the responses of the GRS and HEND, particular

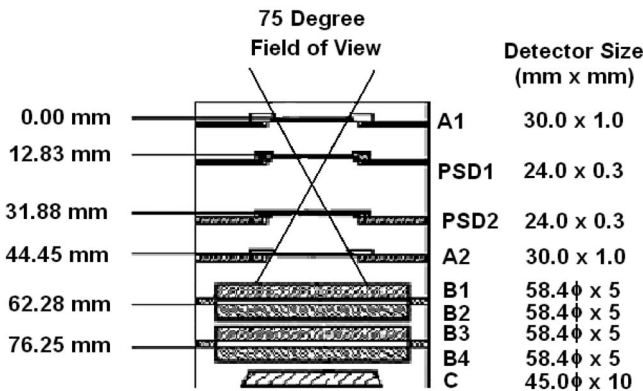


Figure 1. Schematic drawing of the MARIE A, B, and C detectors as seen in a cutaway view from the side.

during SPEs. Third, we present results from the post-MARIE era, up through May of 2008. The data are presented chronologically, and span about half of Solar Cycle 23, from the intense 2002–2003 period through the prolonged minimum. Section 6 discusses the long-term picture of GCR modulation provided by these data and show a comparison of one SPE to EMMREM predictions.

[11] We note that fluxes are often quoted in units of  $\text{cm}^{-2} \text{sr}^{-1} \text{s}^{-1}$ . We refer throughout to this unit as a particle flux unit, or pfu.

## 2. Part I: Instrument Descriptions

### 2.1. MARIE Instrument

[12] MARIE [Badhwar, 2004; Zeitlin *et al.*, 2004] contains a stack of silicon detectors and a Cerenkov detector. The silicon detectors are of three types and sizes: two “A” detectors, square in outline with 3 cm sides and 1 mm in depth; two position-sensitive detectors (PSDs), which are also square in outline with 2.4 cm sides and 300  $\mu\text{m}$  depth; and four “B” detectors, circular in outline with active radii of 2.92 cm and depths of 5 mm. A schematic diagram is shown in Figure 1. Pulse height data were obtained when a particle deposited sufficient energy in both A1 and A2, and these data provide information about particle species and energy. In the present analysis, we rely mainly on counter (“singles”) data from the A1 and A2 detectors.

[13] The only materials between A1 and the vacuum of space are the MARIE case, a 1.27 mm depth of aluminum, and the spacecraft’s thermal blanket, a 100  $\mu\text{m}$  depth of mylar. These materials are sufficient to stop protons and most heavier particles with kinetic energies of about

15 MeV/nuc and below. Protons of energy 16 MeV and above have sufficient range to penetrate as far as A1 with enough energy left over to deposit the (approximately) 1.2 MeV of energy in A1 that is necessary for it to record a hit over threshold with high efficiency. The comparable energy for a proton to penetrate to A2 (and fire the coincidence trigger) is 27 MeV. Readout of the pulse heights of all detectors in the stack was triggered by a coincidence of hits above threshold in the two A detectors. Hits in the single-detector counters did not initiate the pulse height readout, which could digitize only about 3 events per second. Particles incident from the sides can also fire single-detector triggers, but not the coincidence trigger. Shielding of side-entering particles varies by detector.

[14] We noted above that the threshold for efficient triggering in A1 and A2 was about 1.2 MeV, but in reality the thresholds cannot be characterized by a single number since there is not step function behavior. Rather, the trigger efficiency falls for energy deposition below 1.2 MeV, but is greater than zero all the way down to about 0.4 MeV. This means that more energetic particles (which deposit less energy in the detectors) triggered MARIE, but with low efficiency. We base these statements on the measured A1 and A2 spectra, and on the fact that some minimum-ionizing GCR protons are present in the data but in numbers that are far smaller than expected. The observed ratio of high-energy protons to high-energy helium ions in MARIE data is about 1:1, whereas data from other instruments show that the actual ratio is about 7:1.

[15] The nominal geometry factor for MARIE is  $3.19 \text{ cm}^2 \text{ sr}$  for forward going ions that satisfy the A1-A2 coincidence requirement. (Forward going ions are those that strike A1 before A2.) Backward going ions can also fire the coincidence trigger with the same geometry, however, part of the rear FOV is occluded by the disk of Mars. A calculation taking account of the orientation of the telescope with respect to Mars yields a geometry factor of  $2.43 \text{ cm}^2 \text{ sr}$  for the backward FOV. When added to the geometry factor for the forward FOV, we obtain the value of  $5.62 \text{ cm}^2 \text{ sr}$  shown in Table 1. The portion of the rear FOV not blocked by Mars is shielded by various components of the spacecraft, which have a highly nonuniform distribution. Some backward trajectories are heavily shielded, others much less so. The shielding of the rear FOV by various items on the spacecraft introduces considerable complication into the normalization of the GCR data. However, during typical SPE, the shielding stops the large majority of backward going ions. The energy-dependent geometry factor for forward going protons has been calculated [Andersen *et al.*, 2003] and is nearly independent of energy above about 27 MeV.

Table 1. Nominal Geometric Factors for the Instruments Used in This Analysis

	A1 and A2	A1-A2 Coincidence	GRS Ge Detector	HEND Inner Scintillation
G ( $\text{cm}^2 \text{sr}$ ) Efficiencies	41.3 Shielding, threshold	5.62 Shielding, threshold, dead time	941.5 Chord distribution, dead time	238 $p + X \rightarrow n$

[16] Counts above threshold in detectors A1, A2, B2, and B4 were summed and recorded once per minute. In practice, the nominal 1 min intervals were unequal due to housekeeping tasks being performed by the CPU on a 5 min cycle. This resulted in one of every five intervals being slightly longer than a minute, and one in five being shorter by the same amount. Accordingly, the data must be summed over 5 min intervals to get an accurate reading of counts per unit time. The maximum count rate per minute is 65535, after which the counter rolls over to 0. The maximum flux corresponding to this rate is about 26 pfu for A1 and A2. In a few instances of intense SPEs, rollovers were observed in the A1 counter. For the most part, rollovers are obvious, and one can simply add back in the missing number of counts. Having the A2 counts is helpful, since the A1/A2 count ratio tends to vary slowly over the course of an event and the addition of the missing counts tends to restore the ratio to its correct value. In a very small number of cases, it appears the A1 counter rolled over twice, based on the A1/A2 ratio.

## 2.2. Gamma Ray Spectrometer

[17] The Gamma Ray Spectrometer suite of instruments [Boynton *et al.*, 2004] consists of the gamma ray detector itself (made of high-purity germanium, or HPGe), the Neutron Spectrometer, and the High Energy Neutron Detector. The germanium crystal is referred to as the Gamma Sensor Head, or GSH. All detectors in the GRS suite share a common readout through the GRS Central Electronics Box (CEB). The HPGe detector is mounted on a 6 m long boom in order to greatly reduce the contamination of the spectra from gamma rays that are produced in the spacecraft. It is a right-circular cylinder, with diameter and length both equal to 6.6 cm, with an operating temperature below 90°K. Its primary purpose is to measure gamma rays with energies as low as a fraction of an MeV up to several MeV.

[18] The HPGe crystal needs to be large in order to contain the full energy of the gammas, and also because the flux of gammas from the Martian near subsurface is fairly small. This makes the crystal a large target for energetic charged particles, both GCR particles and solar energetic particles. For this reason, the readout electronics contains dedicated circuitry designed to handle the energy depositions from energetic charged particles that traverse, or stop in, the crystal. These are much larger than typical energy depositions from gamma rays. When the energy deposition exceeds 11.8 MeV, the upper level discriminator (ULD) fires, and the ULD counter is incremented. These signals are not pulse height analyzed. Despite the lack of pulse height information, the ULD count rate is an extremely useful, direct measurement of the incident flux of energetic charged particles. The ULD counter can record up to 65535 counts in a single measurement interval.

[19] The minimum proton energy required to fire the ULD appears, based on SPE data, to be about 42 MeV. This is estimated from examining five SPEs in 2002 where

we have integral fluxes from the ULD and from the MARIE A1 and A2 counters. The Ellison-Ramaty form [Ellison and Ramaty, 1985] for  $dJ/dE$  and double power law forms were both tested against the data by varying the free parameters until reasonable agreement was found. With either type of fit, the results are most consistent with a ULD threshold of 42 MeV. This is not the actual energy deposition required; that value is 11.8 MeV. The relatively high threshold is due to the fact that the HPGe crystal is embedded in a passive radiative cooling structure, and is for the most part under considerable shielding (see Figure 2 of Hurley *et al.* [2006]), with the exception of the end of the cylinder that points away from Mars, which is shielded only by the detector housing. Given the geometry of the cooler assembly and the fact that the solar beta angle was restricted to angles smaller than -55° (to keep the GRS cooler pointing away from the sun), this end of the cylinder could point parallel to the plane of the ecliptic but could never point into the Parker spiral line that connects Mars to the sun. (As further proof of this statement, there were no enhancements in fluxes as Odyssey passed through the ecliptic during solar energetic particle (SEP) events.)

[20] Gaps in the ULD time record occurred when the HPGe crystal was annealed (typically following a space-craft safe-mode entry) and as a result of the deployment of the GRS boom in mid-2002.

## 2.3. High Energy Neutron Detector

[21] The High Energy Neutron Detector [Boynton *et al.*, 2004], built by the Russian Space Science Institute, consists of five separate sensors, each sensitive in a different range of neutron energies. Three of the five sensors are  $^3\text{He}$  tubes, which detect neutrons via a nuclear capture reaction. The other two sensors, including the one of particular interest for indirect energetic charged particle measurements, comprise the Scintillator Block (SC), which consists of two scintillators, an inner stilbene crystal surrounded by an outer cesium iodide (CsI) detector. Stilbene is an efficient neutron detector because it is hydrogenous ( $\text{C}_{14}\text{H}_{12}$ ). The CsI provides a veto signal when the SB is struck by a charged particle. A neutron event is defined as the presence of a hit in the stilbene and the absence of a hit in the CsI. However, relatively high energy recoil protons from neutron reactions in the stilbene can also produce a hit in the CsI, limiting the upper energy at which the system is efficient to about 10 MeV. The lower limit of neutron sensitivity is 300 keV. Pulses from the stilbene are pulse height analyzed by a four-bit analog to digital converter (ADC). In data processing for NASA's Planetary Data System (PDS), hits are totaled in two bins, the "low" and "high" channels, corresponding to ADC channels 1–4 and 5–16, respectively; we use the latter here. The stilbene is surrounded by a CsI anticoincidence shield and hence is referred to as the inner scintillator. Thus a useful acronym for this channel is "SCIH," for Scintillator Inner High.

[22] A considerable fraction of the neutrons recorded in the SCIH are produced in Odyssey itself when high-energy cosmic rays interact with various pieces of the spacecraft; this is a large background, on top of which sits the signal of interest, i.e., the flux of high-energy neutrons coming from Mars. These are also formed by interactions of charged particles, in the Martian soil and atmosphere. The HEND team use the data obtained during Odyssey's cruise to Mars to estimate and subtract the contribution to the count rates from neutrons produced in the spacecraft. A time-dependent correction is applied to account for the varying fraction of the solid angle subtended by Mars as the spacecraft orbits as well as for variations due to the solar cycle. Thus, in the Derived HEND Data (DHD) used in the present analysis, the "adjusted" counts during solar quiet time are due to neutrons coming from Mars. The neutrons coming from the spacecraft are, for present purposes, a large part of the interesting signal, so we have chosen to use the "raw" counts. This improves both the statistical accuracy and systematic accuracy of the data, at the price of including subtle count rate oscillations due to Odyssey's slightly elliptical orbit. During SPEs, the flux of neutrons produced in the spacecraft increases. (The flux of neutrons coming from Mars also increases, but less dramatically.) The HEND team specifically flags the data in the DHD product, used in this analysis, so that users are aware of SPEs and can avoid using those data for studies of Martian surface properties.

[23] During solar quiet time, when the incident GCR spectrum is approximately constant (varying on time-scales of months or years), and integrating over sufficiently long time periods, the neutron spectrum seen in the SCIH channel maintains a roughly constant shape, leading to a steady count rate. In contrast, energy spectra of solar protons can vary substantially between events. The neutron flux depends on the incident proton spectrum, so that the response of the SCIH during various solar events is not simple when compared to other instruments. For instance, for 2002–2003, where MARIE data are available, during SPEs it was invariably observed that (relative to quiet time) the MARIE A1 count rate increased more than did A2, and A2 increased more than the ULD. In contrast, at various times HEND count rates are observed to increase at about the same rate as A1, or A2, or the ULD, and in some events to increase at a rate even less than that of the ULD. This complexity makes interpretation of the data difficult, but also raises the possibility that, even in the absence of spectral information from MARIE, some rough characterization of the incident spectrum may be possible.

### 3. Geometry Factors and Normalization

[24] Many useful formulas for the calculation of geometry factors,  $G$ , have been compiled by *Sullivan* [1971]. In the simplest case, a single detector of area  $A$  in free space with an isotropic flux of particles,  $G = 2\pi A$ . The calculation of  $G$  depends on the assumed angular distribution of the

flux, which we take in all cases to be isotropic, though this may not be a good approximation during SPEs, particularly near the onset.

[25] In Odyssey's orbit, Mars subtends a significant fraction of the  $4\pi$  solid angle from which energetic particles can reach a detector. The fraction varies slightly with time because the orbit is not perfectly circular. The maximum solid angle subtended (at perihelion) is about 27.8% of  $4\pi$ , the minimum 26.4%. On average about 27% of  $4\pi$  is blocked by Mars, so to first-order  $G = 1.46\pi A$  for the case of a single detector and an isotropic source. Table 1 shows nominal geometry factors for the detectors used in this study. We emphasize that these are purely based on geometry and the shadowing of the detectors by Mars, and do not take account of additional complicating factors.

[26] For a realistic detector capable of measuring fluxes in well-defined energy bins, the differential flux is given by

$$\frac{dJ}{dE} = \frac{N_E}{G\Delta t\Delta E\varepsilon(E, Z, A)} \quad (1)$$

where  $N_E$  is the number of counts accumulated in a time interval  $\Delta t$  in an energy bin of width  $\Delta E$  centered on energy  $E$ , with efficiency  $\varepsilon(E, Z, A)$  a function of the energy ( $E$ ), charge ( $Z$ ), and mass ( $A$ ) of the incident particles. The efficiency  $\varepsilon$  can be absorbed into the definition of  $G$ , i.e.,  $G = G(E, Z, A)$ . Since the data presented here are derived from count rates with no identification of particle type or energy, we present only integral fluxes with various low-energy thresholds. These are simply integrals of equation (1), with lower limits for the integrations determined by the detector sensitivities.

#### 3.1. Saturation of Counters in MARIE and GRS Data

[27] The A1, A2, and ULD counters all roll over when they reach 65535 counts in a given measurement interval. As mentioned above, for A1 and A2, the peak flux before rollover is 26.4 pfu; for ULD, with 19.76 s intervals and a much larger geometric factor, the peak flux is 4 pfu. In the data acquired to date, there is no evidence of rollovers in the SCIH data.

#### 3.2. Efficiencies

[28] The MARIE detectors and the GRS germanium crystal have readily calculable geometric factors and reasonably straightforward detection efficiencies. Likewise,  $G$  can be calculated for the SCIH, but it has a very complex efficiency since it records a secondary neutron flux that depends on the interactions of charged particles. The count rates recorded by the different devices vary widely, with the ULD recording by far the highest rates and the SCIH by far the lowest. The detectors also have different sensitivity as determined by the threshold energy for protons to register, about 16 MeV for A1, 27 MeV for A2, and 42 MeV for ULD as described above. The thresholds for MARIE A1 and A2 are based on straightforward energy loss calculations. Because of the complexity of the

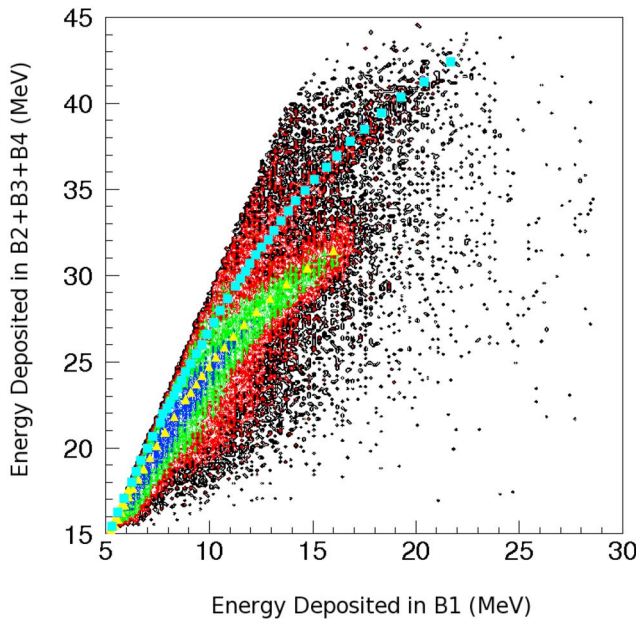


**Figure 2.** MARIE pulse height data from January 2003 when no SPEs were observed at Mars. The sum of deposited energy in detectors B2, B3, and B4 is plotted against the deposited energy in B1. The light blue squares show predicted energy losses for deuterons, and the yellow triangles show protons.

SCIH response, it cannot be characterized by a simple threshold. For most of the SPEs recorded by MARIE, the SCIH tracks reasonably well with the A2 counter.

[29] A detailed discussion of the rear MARIE field of view is given in Appendix B. To briefly summarize, despite the shielding and the shadowing by Mars, a considerable flux of backward going ions entered the detector and fired the coincidence trigger, but these were generally high energy particles not associated with SPEs. They are an approximately constant, continual source of background in the MARIE data. As mentioned above, the telescope has a geometry factor of about  $2.43 \text{ cm}^2 \text{ sr}$  for backward going ions. The average shielding in this FOV is about  $25 \text{ g cm}^{-2}$ . A proton must have energy of at least 170 MeV to penetrate  $25 \text{ g cm}^{-2}$  of aluminum. Typical SPEs have energies well below 100 MeV. We conclude that the flux of solar protons that entered MARIE from the back of the telescope and fired the A1-A2 coincidence was negligible. On the other hand, a high percentage of GCR protons and helium ions have energies above 170 MeV/nuc and can therefore penetrate the rear shielding mass and reach A1. In MARIE pulse height data, relatively low energy backward going protons and deuterons are seen, as illustrated in Figure 2. Deuterons are rare in the GCR; they are generally believed to be dominantly secondaries. The considerable flux of them seen in the MARIE rear FOV is almost certainly due to nuclear interactions of high-energy ions that enter the

spacecraft. In summary, the nominal geometry factors for MARIE are easily calculated, but the efficiency is complicated due to the rear FOV shielding and the poorly understood trigger threshold.

[30] A simple efficiency correction to the ULD flux is needed based on geometry. The ULD fires whenever an energy deposition greater than 12 MeV is recorded in the germanium crystal. Given the size and density ( $\rho = 5.3 \text{ g cm}^{-3}$ ) of the crystal, a minimum-ionizing proton that passes through it with a chord length equal to the crystal's diameter will deposit approximately 50 MeV of energy. Therefore protons, and heavier particles, with chord lengths of at least 24% of the crystal's diameter will be recorded as hits in the ULD. The chord length distribution for isotropic radiation entering a cylinder has a most probable value equal to the cylinder's diameter, with a large tail to shorter chord lengths. The HPGe crystal does not see a random distribution of incident particles due to shadowing by Mars. The crystal's axis points  $17^\circ$  off of the nadir/zenith line, so that trajectories nearly parallel to the axis (i.e., long path lengths) are preferentially blocked. A detailed calculation shows that, for trajectories not blocked by Mars, approximately 15% of the chord length distribution corresponds to lengths less than 24% of the diameter. Therefore, to first order, the ULD should be about 85% efficient at recording protons, and more efficient than that for heavier particles such as helium. Since the flux is expected to consist dominantly of protons, this correction factor ( $= 1/0.85$ ) has been applied to obtain the results shown below.

[31] It is not surprising that (as will be shown), the flux recorded by the SCIH channel is far lower (by a factor of 28) than the fluxes from the GRS and MARIE due to the indirect nature of the measurement. The SCIH flux is scaled up by this factor in all of the subsequent analysis. This is an *ad hoc* correction based on the response to the GCR spectrum at a particular time, and it should be borne in mind that it may not be accurate under all circumstances.

### 3.3. Normalization of GCR Rates

[32] An important reference point for the integral GCR flux in this time period comes from data obtained at 1 AU. The GCR radial gradient is small in the inner heliosphere, so that the flux at Mars is expected to be the same as at 1 AU to a good approximation. Data taken in 2002 by ACE/CRIS [George *et al.*, 2009] and BESS [Shikaze *et al.*, 2007] yield an estimate of about  $0.16 \text{ cm}^{-2} \text{ sr}^{-1} \text{ s}^{-1}$  for the integral GCR flux including electrons (R. A. Mewaldt, private communication, 2010). Normalization of the Odyssey data are done using samples from mid-2002, so the results should be directly comparable.

[33] Count rates were studied for a 10 day quiet period in 2002, days 180 through 189. During this time, all counters recorded nearly constant rates and all were in stable configurations that would remain throughout the mission. Previously, the GRS boom had been deployed and the crystal had been recently annealed, and on day

**Table 2.** Average Rates for Days 180–189 of 2002<sup>a</sup>

	A1	A2	A1-A2 Coincidence	GRS ULD	SCIH
Counts/interval Flux ( $\text{cm}^{-2} \text{ sr}^{-1} \text{ s}^{-1}$ )	$602 \text{ min}^{-1}$ 0.243	$503 \text{ min}^{-1}$ 0.203	$45.4 \text{ min}^{-1}$ 0.135	1828 0.116	7.07 0.0016

<sup>a</sup>The GRS and HEND time intervals were 19.76 s.

122, threshold settings for the MARIE A1 and A2 counters were adjusted to their final values. Table 2 shows the count rates and corresponding fluxes, obtained using nominal geometric factors and only a single correction of about 18% applied to the GRS result to account for the effect of the cylindrical chord length distribution and the 12 MeV ULD threshold. The MARIE counter fluxes are larger than that determined by the coincidence trigger. As expected, the A1 flux is largest, since it sees lower-energy particles than does A2. Because A2 is much more shielded than A1, the A2 flux should agree with the flux obtained from the coincidence geometry. However, for reasons discussed below, the two do not agree.

[34] The difference between the A1-A2 coincidence flux and the A2 counter flux suggests that there likely was a constant contribution to the A2 counts (and presumably the A1 counts as well) from electronic noise. This, in fact, is the reason for having a coincidence trigger; a coincidence eliminates (or at least decreases) noise triggers from single detectors with low thresholds. Thus the coincidence flux is the more credible result. However, given that the thresholds were relatively high, we estimate that only 30%–35% of GCRs triggered MARIE. If we apply a factor of 3 correction to the flux obtained by counting coincidence triggers with no cuts on the data, we find a value of about  $0.4 \text{ cm}^{-2} \text{ sr}^{-1} \text{ s}^{-1}$ . This is far in excess of what we believe to be the actual flux based on the ACE/CRIS and ULD results. The result is difficult to understand; it implies that either (1) the coincidence trigger was also plagued by noise or (2) the trigger efficiency was much larger than we believe (and the effective threshold lower) but the pulse height circuitry systematically corrupted events with small deposited energies.

[35] In the face of these difficulties, we have devised another means of estimating the integral GCR flux from the coincidence-triggered data. First, we select events consistent with high-energy helium ions (for which we expect the trigger efficiency was close to 100%) and apply efficiency corrections as determined by Monte Carlo calculations. We divide by the nominal geometry factor to obtain the total He flux and then extrapolate the result to the integral flux for all species using the ratio of total flux for all species to the helium flux as predicted by the Badhwar-O'Neill GCR model (7.8:1). This method yields a value of  $0.15 \text{ cm}^{-2} \text{ sr}^{-1} \text{ s}^{-1}$ , which is in good agreement with the ACE/CRIS result and also more believable than the result obtained by simply counting coincidence triggers.

[36] Averaging the MARIE coincidence flux based on He with the ULD result, we obtain an integral GCR flux of

$0.133 \text{ cm}^{-2} \text{ sr}^{-1} \text{ s}^{-1}$ . Since we believe the A1 and A2 counters were affected by noise, in the following, we make another *ad hoc* correction by subtracting a flux of  $0.07 \text{ cm}^{-2} \text{ sr}^{-1} \text{ s}^{-1}$  from both. This brings the A2 counter flux into agreement with the averaged MARIE coincidence and ULD flux. The correction to the A1 counter data is based on the fact that the thresholds had identical settings, and on the assumption that the detectors had similar noise levels; there is no way to independently verify this. The SCIH data are also normalized so this same quiet time value ( $0.133 \text{ cm}^{-2} \text{ sr}^{-1} \text{ s}^{-1}$ ) by multiplying the neutron flux by a factor of 89.8.

[37] These GCR fluxes are significantly lower than predicted by the Badhwar-O'Neill model for the 2002–2003 time frame. The model code yields differential fluxes for all species from H to Ni. Integrating each species over energy and adding the per species fluxes yields a prediction of  $0.249 \text{ cm}^{-2} \text{ sr}^{-1} \text{ s}^{-1}$ , nearly a factor of 2 higher than seen by the Odyssey instruments and 50% higher than the ACE/CRIS estimate. The quiet time normalization is not critical for the study of SPEs, since the GCR fluxes are subtracted from the fluxes seen in the events.

#### 4. Part II: Results From 2002 to 2003, Intercalibration

[38] As noted at the outset, we have MARIE data only from March 2002 through October 2003, while GRS and HEND data are both available through late 2008. It is therefore desirable to make use of the SPE data obtained while MARIE was operating to understand the GRS and HEND responses during events. Specifically, we compare the responses of the A1 and A2 counters (with reasonably well known thresholds determined by energy loss calculations) to those of the GRS ULD and HEND SCIH. Several solar events were observed by MARIE during its short operational life. A few small, soft-spectrum events seen in the A1 counter did not register in the ULD and SCIH channels, and barely registered in A2.

##### 4.1. Observations From March 2002 Through December 2002

[39] Figure 3 shows the A1 and ULD fluxes for 2002 with 5 min time binning. The large geometric factor of the ULD produces very high statistics data. The GRS data have fewer gaps than MARIE.

[40] MARIE was mostly off for the month of August 2002. There was also a significant outage for all channels from day 310 to day 318 due to a spacecraft safe-mode entry and subsequent recovery. This was followed on days

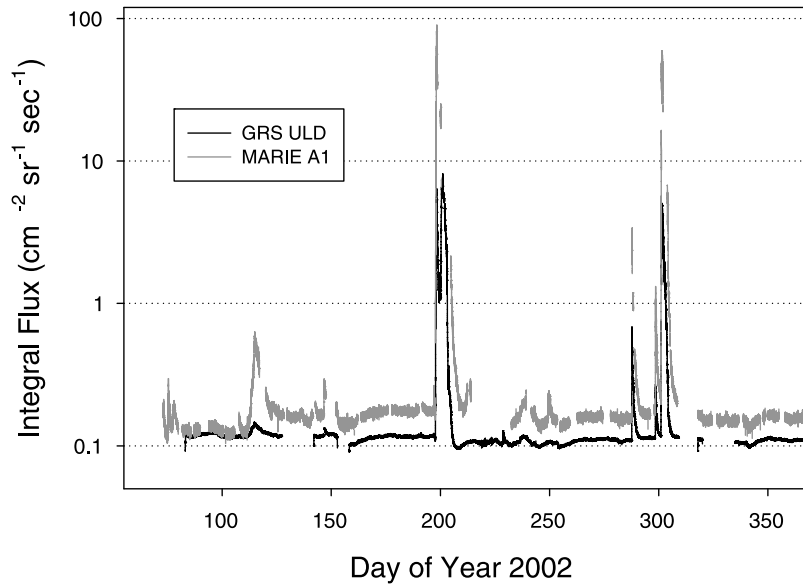


**Figure 3.** Integral fluxes for 2002 as measured by the MARIE A1 counter (gray line,  $E_{proton} > 16$  MeV) and by the GRS ULD (black line,  $E_{proton} > 42$  MeV.)

320–332 by a GRS outage for annealing. We will return to further comparisons of MARIE and ULD data below.

[41] Figure 4 is similar to Figure 3, but showing SCIH instead of ULD in comparison to A1. HEND's time coverage is the best of the channels studied here. However, for reasons described above, the statistics are comparatively poor. The MARIE threshold decrease and corresponding rate increase starting at day 122.8 is clearly visible here.

#### 4.1.1. Days 110–128, 2002

[42] A small, soft SPE is seen starting on day 112, as shown in Figure 5. The peak flux seen in A1 reached 0.64 pfu at day 114.9. The peak flux in A2 was about one-third as large as in A1, and in the ULD the maximum flux was about 0.15 pfu, only very slightly above the quiet time level. The GRS boom had not yet been deployed, so the sensor head was more shielded at this time than it was subsequently. The SCIH recorded a peak of about 0.2 pfu, similar to ULD and again only slightly above the quiet

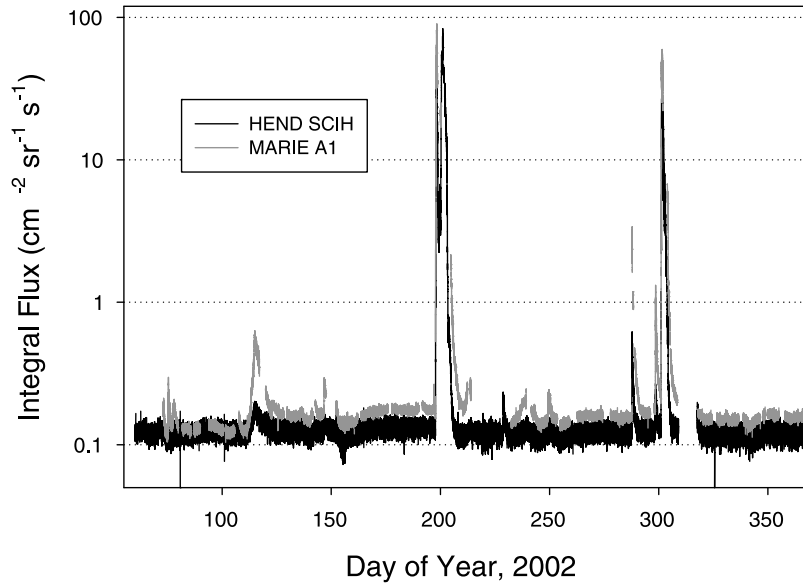


**Figure 4.** Integral fluxes for 2002 as measured by the MARIE A1 counter (gray line) and by the HEND SCIH (black line).

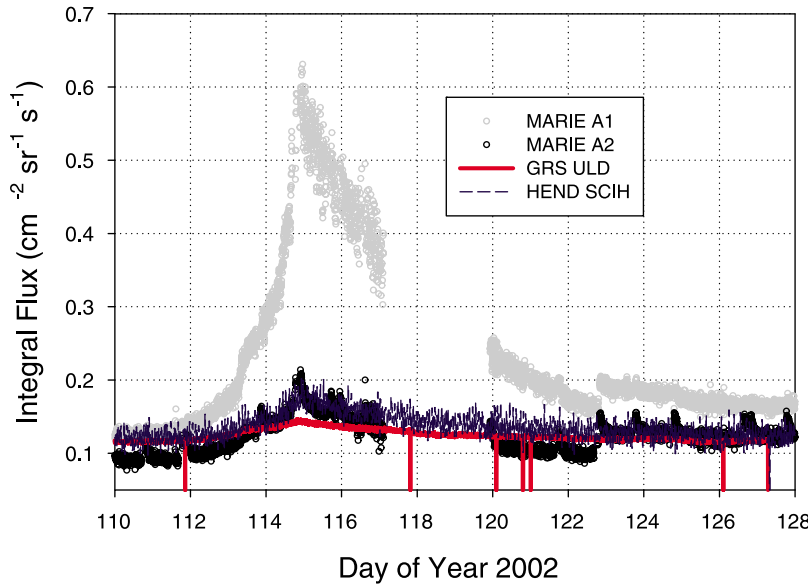


**Figure 5.** Integral fluxes for days 110–128 of 2002 as measured by the MARIE A1 counter (open gray circles), the A2 counter (open black circles), HEND SCIH (blue line), and by the GRS ULD (red line).

time rate. Though not a significant event, it is illustrative of the typical behavior shown by the four channels. This event occurred prior to the final adjustment of the A1 and A2 threshold adjustment, the effects of which can be seen starting at about day 122.8. Note that the small upward excursions seen in the A2 channel (e.g., at 122.9, 123.9, etc.) invariably followed the instrument being power cycled; this behavior was apparently caused by temperature dependence in the A2 comparator circuit, resulting in a short-lived lower effective threshold after the instrument was turned on.

#### 4.1.2. Days 195–215, 2002

[43] A full-halo CME as seen from Earth (SOHO at L1) occurred on day 196 (15 July), with the first indication being an X-ray flare observed by GOES starting at about 2000 UT. Mars at this time was nearly on the opposite side of the sun from the Earth (which was leading Mars by 167° in heliocentric longitude), and about 1.64 AU from the sun (near aphelion). The first SEPs to arrive at Mars can be seen near day 197.0 in the MARIE A1 and ULD channels, followed by a decreasing flux for about 12 h, after which

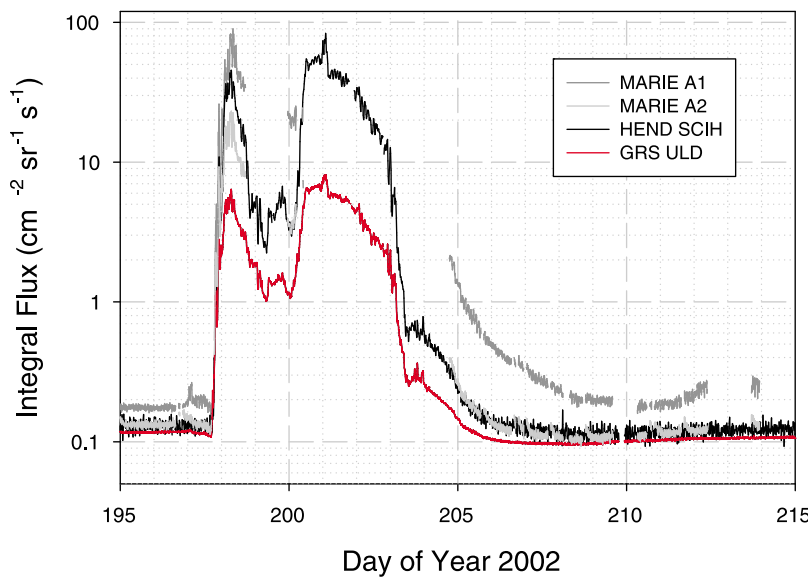


**Figure 6.** Integral fluxes for the large July 2002 SPE as seen at Mars.

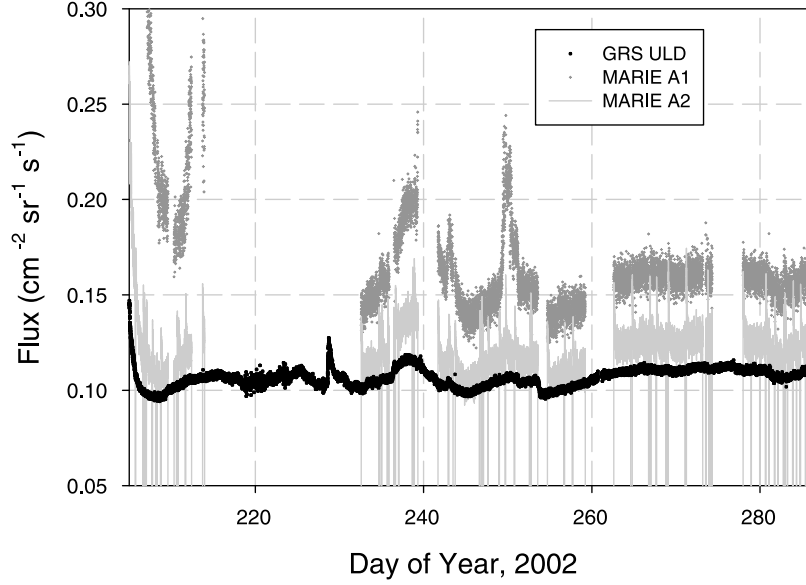


**Figure 7.** Fluxes seen by the A1, A2, and ULD channels for days 205–286 of 2002.

time the flux in all counters rose dramatically. (Note that there is an excursion in the A2 rate at about day 196.7; this is not an indication of solar activity, rather it is related to the threshold shift invariably seen after power cycling, discussed in section 4.1.1.) The high data rate caused MARIE to halt acquisition fairly soon after energetic particles began arriving, but the first peak was captured, as can be seen in Figure 6. The peak fluxes for A1, A2, SCIH, and ULD at day 198.34 were 90, 22, 34, and 6.4 pfu, respectively. In this instance, the SCIH flux was higher than that of A2, starting at 198.05 and continuing until MARIE stopped acquisition at 198.72. This is likely indicative of a particularly soft energy spectrum, as will be explained further in the following. There are no good MARIE pulse height data from this event due to the high rate. The ratio of A1 flux to ULD flux was about 14 at the peak; during the brief MARIE up time around day 200, the ratio was somewhat higher, 16.6 on average. For A1/A2, the ratios were 4.1 at the peak and an average of 5.6 for the day 200 uptime. The A1/A2 and A1/ULD ratios are rough indicators of spectral hardness, and the increased ratios suggest a softening of the spectrum as the event progressed. The MARIE data cannot be integrated due to the lack of coverage, but the integrated SCIH flux from day 197.7 to day 205.8 is about  $2 \times 10^5 \text{ cm}^{-2}$ , about five times larger than the integrated ULD flux over the same time.

[44] By day 210, the A2, SCIH, and ULD fluxes had all returned to quiet time levels, but the A1 flux remained at a slightly elevated level and in fact rose between about day 211 and 212.5, when MARIE ceased acquisition. MARIE was on only briefly on day 213 (and then off until day 232), but the continuing elevation in A1 persisted.

#### 4.1.3. Days 205–286, 2002

[45] Figure 7 shows the A1, A2, and ULD fluxes from day 205 to day 286. The SCIH data are not shown here as they generally followed the ULD data, with the exception of day 228. On that day, a small SPE was seen, reaching its peak at about day 228.8. The peak ULD flux was about 0.125 pfu, barely above the quiet time level due to GCR, while the peak in the SCIH channel was somewhat higher, about 0.23 pfu. Another small event is seen 11 days later, with A1 reaching a peak of 0.25 pfu at 239.2. Very slight flux increases are seen in the A2, SCIH, and ULD data. Small events are also seen in A1 on days 239, 243, and 249–250, with little or no visible increases in the other channels.

[46] A modest Forbush decrease can be seen in the ULD data following the solar activity that began on day 197 (see Figure 6). The ULD flux reached a minimum of about 0.095 pfu, roughly 20% lower than the flux just prior to the event. After the Forbush decrease, GCR quiet time levels did not return to their previous level, and additional small dips can be seen on days 251 and 254. After day 254, the GCR flux as seen by the ULD rose steadily, but remained about 5% below the average flux from day 180 to day 190.

#### 4.1.4. Days 285–365, 2002

[47] Figure 8 shows all four channels for days 285–310 (12 October to 6 November). Three SPEs occurred, with the final one being the largest, peaking on day 301. In the first two events, A1 and A2 recorded significantly higher fluxes than the other two channels. However, in the largest event, the SCIH flux is higher than that in A2 by a factor of 1.5–2 near the peak of the event.

[48] In Figure 9, we plot the ratios of the other counters relative to the A2 counter for the two later events in this period. Here, data points are plotted only when the A2

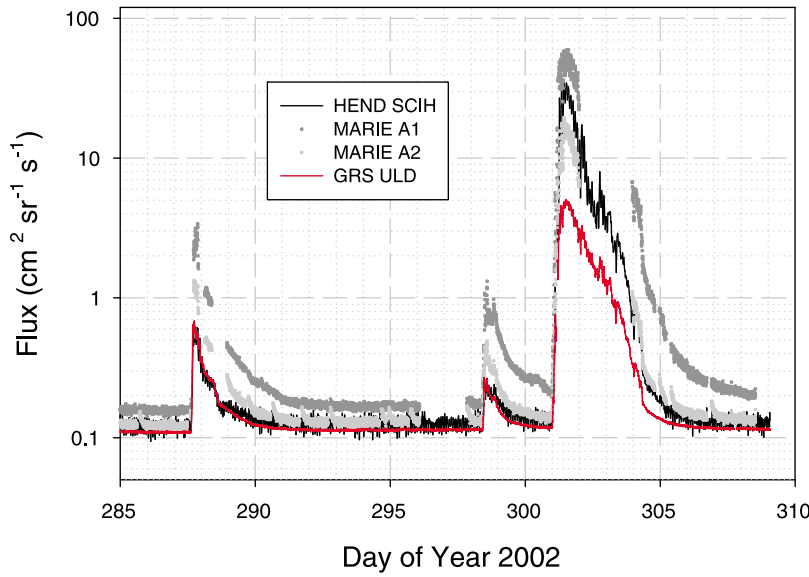


**Figure 8.** Fluxes during the solar particle events of October 2002.

flux exceeded twice its quiet time level, and for all channels, the quiet time flux has been subtracted, so the plotted quantities are the ratios of SEPs seen in the different channels. The A1/A2 ratio should be an indicator of event hardness, and we note that at the onset of the first event, the ratio was about 1.7 and quickly rose to values greater than 2. At the same time, the ULD/A2 ratio dropped from 1 (very close to the quiet time ratio) to about 0.45, where it remained for the remainder of this brief, weak event. These time dependencies may relate to the earlier arrival

of the more energetic particles. The SCIH/A2 ratio during this time remained in the 0.15–0.7 range, with considerable scatter, possibly due to counting statistics in SCIH.

[49] In the larger event which began on day 301, the A1/A2 ratio is again seen to rise quickly to levels above 2. The ULD/A2 ratio remains in the 0.2–0.6 range. Orbit-related oscillations are visible in this ratio, and appear more prominently in the count rates; the oscillations and their underlying cause are described elsewhere [Luhmann *et al.*, 2007]. The SCIH/A2 ratio starts off at about the same level

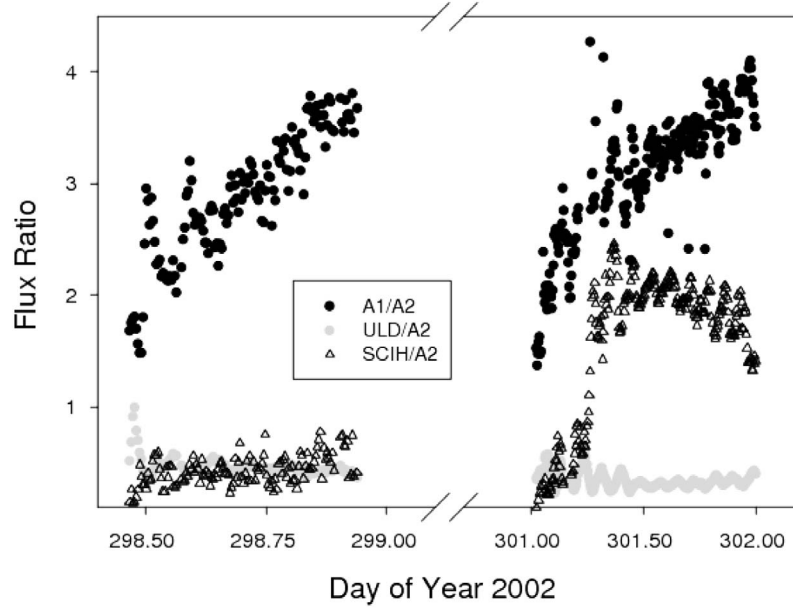


**Figure 9.** Fluxes relative to the A2 counter during the solar particle events on days 298–302 of 2002.

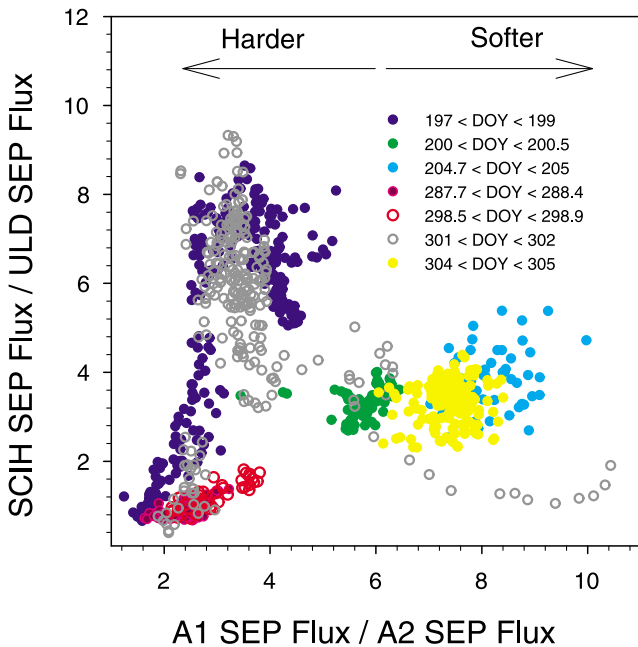


**Figure 10.** SCIH/ULD ratio versus A1/A2 ratio for data obtained during SPEs in 2002. Background GCR fluxes have been subtracted from all channels.

as at the end of day 299, but around 301.25 it suddenly increases to the 1.7–2.4 range. The trend of the A1/A2 ratio indicates a gradual softening of the spectrum in the 15–27 MeV range, while the ULD/A2 ratio suggests a more nearly constant flux in the 27–42 MeV range. Seen in this light, the cause of the SCIH/A2 ratio increase is not obvious. It is conceivable that the SCIH/A2 increase corresponds to a major increase in the flux of SEPs below the A1 threshold, i.e.,  $E_{proton} < 16$  MeV. GOES data from this period do not show any sign of SEPs, however Mars was leading Earth by about  $170^\circ$ , so an active region on the sun that was magnetically connected to Mars would not have been connected at Earth. Four days later, on 31 October (day 304), GOES recorded the start of an increase in its  $>10$  MeV proton channel, eventually peaking at 1 pfu and persisting above quiet time levels for about 6 days. No increases are seen in the GOES  $>30$  MeV channel for that time.

[50] For the remainder of 2002, no other SPEs were seen following the event that peaked on day 301. In November, Odyssey experienced a safe-mode entry, leading to an outage for all instruments from day 309 to day 317. Successful annealing of the GRS HPGe crystal followed, with normal operations resuming on day 335.

#### 4.1.5. SEP Flux Ratios in 2002 Data

[51] It is useful to examine the solar events observed with all four channels available. For times subsequent to the MARIE failure, only the ULD and SCIH channels are available. Since the A1/A2 ratio is an indicator of spectral hardness for proton energies above 15 MeV, it is worthwhile to investigate whether the SCIH/ULD ratio might

(fortuitously) show correlation with the A1/A2 ratio during solar events. Figure 10 shows a cross plot of the ratios with GCR quiet time rates subtracted in all channels. The results are intriguing but not single valued. For A1/A2 SEP ratios below about 6, there does indeed seem to be a strong positive correlation with the SCIH/ULD ratio, suggesting that during SPEs the SCIH is quite sensitive to the flux of low-energy protons, likely including those below the A1 threshold. However, for A1/A2 ratios above 6, the SCIH/ULD ratio is considerably lower than it is for lower A1/A2 ratios. Almost all of the data with large A1/A2 ratios are seen on days 204 and 304, after SPE peaks on days 201 and 301, respectively. Therefore, we can make the following observations about the correlation of ratios: (1) SCIH/ULD ratios below 2 typically correspond to A1/A2 ratios below about 3.5; (2) SCIH/ULD ratios above 5 correspond to A1/A2 ratios from about 2.5 to 5; and (3) SCIH/ULD ratios in the 2–5 range correspond to A1/A2 ratios above 5. In the SPEs considered here, we do not see any in which the flux of SEPs measured by the ULD exceeded that measured in SCIH. In section 4.2, the 2003 results are examined, and these tentative conclusions are further explored.

#### 4.2. Observations From January 2003 Through October 2003

[52] Odyssey data for 2003 are available except for the time during and immediately after the very intense, well-known Halloween event. The event caused a spacecraft safe-mode entry on day 301 (28 October). Science operations resumed on day 310 (6 November), at which time it was discovered that the MARIE instrument was nonresponsive. Recovery attempts continued throughout 2003 and 2004 with no response, and were finally abandoned. The GRS HPGe crystal required annealing after the October spacecraft safing, and GRS data taking resumed on day 331. Prior to the large October event, only a couple of comparatively small SPEs were observed.

##### 4.2.1. Days 1–83, 2003

[53] Days 1 through 76 of 2003 were quiet. Some minor variations are seen, but ULD count rates were stable to within  $\pm 10\%$  over this period. A small SPE began on day 77 and continued until day 80. Figure 11 shows the details. Fluxes in A1 and A2 peaked at 1.4 and 0.4 pfu, respectively, though the peak of the event was apparently missed by MARIE due to an outage while data were uploaded to the spacecraft. The orbit-related oscillations were particularly strong in this event (see Luhmann *et al.* [2007] for more details), and can be seen in the ULD for the portions of the event where the ULD flux was above about 0.16 pfu. The SCIH at this time was showing oscillations that appear to be orbit related at all times including during the SPE, however these were not necessarily in phase with those recorded in the other channels. The A1 and A2 oscillations end when the fluxes return to quiet time levels. The excursion of the A2 flux at day 81.8 is due to the comparator issue described above; it is perhaps more prominent in this view because the horizontal axis has

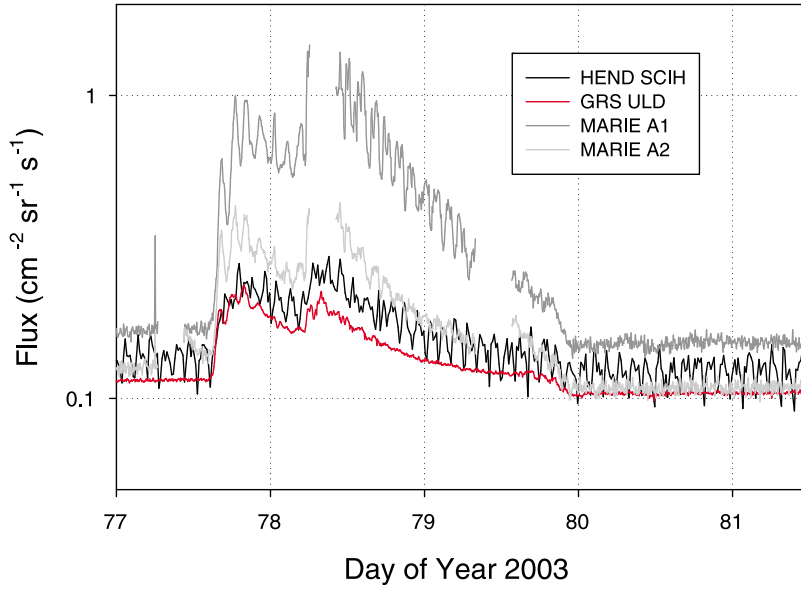


**Figure 11.** Fluxes for the SPE in March 2003 as measured by the A1, A2, SCIH, and ULD channels.

been expanded compared to plots shown previously. The SCIH and ULD fluxes are quite close to one another throughout this event, and the A1/A2 SEP ratio is typically between 2 and 3, so that these data would populate the lower left-hand corner of Figure 10.

#### 4.2.2. Days 83–157, 2003

[54] Days 83 through 148 were quiet in all channels. As can be seen in Figure 12, the A1 flux began a gradual rise from about 0.17 pfu to 0.20 pfu on day 148. An extremely short lived peak is seen at day 149.9 but only in A1; the A2

increase at this time is a comparator-related artifact. ULD and SCIH fluxes start to decrease at 150.1, at which time another brief increase is seen, again only in A1, lasting only until 150.2. All channels see SEPs starting at 151.1. The ULD flux briefly rose above that seen in SCIH, but for most of the event the two are very close. This is consistent with a hard energy spectrum.

#### 4.2.3. Days 157–290, 2003

[55] No solar events were seen in this period. The GCR flux rose slightly in the A1, A2, and ULD channels,

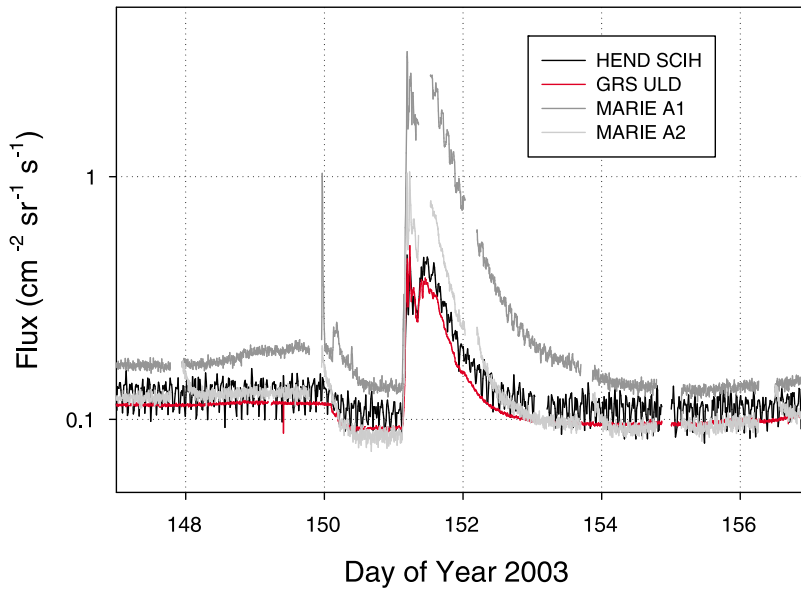


**Figure 12.** Integral fluxes for days 147–157 of 2003.

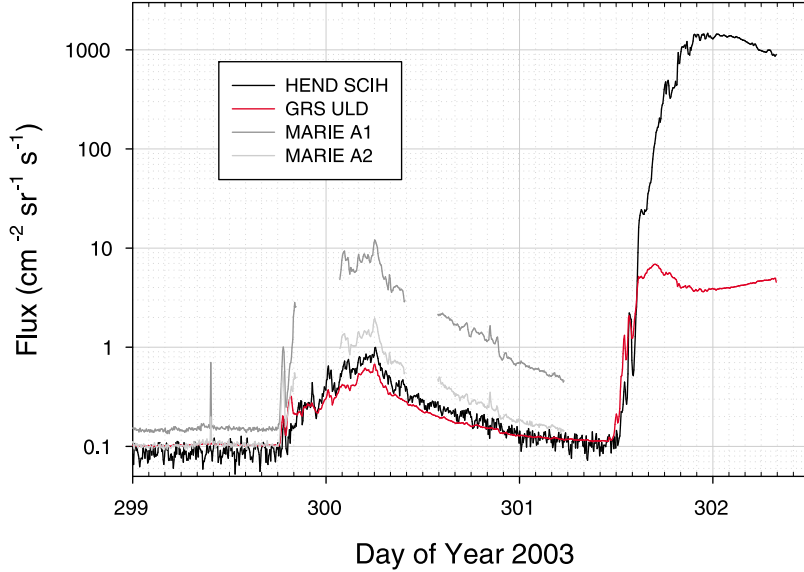


**Figure 13.** Fluxes just prior to the Odyssey safe mode during the Halloween event of 2003. Data from the Mars Global Surveyor (MGS) Electron Reflectometer for the Halloween 2003 SPEs, also showing the last data collected by the HEND SCIH channel before the Odyssey safe-mode entry.

increasing by about 17%, 19%, and 10%, respectively, for days 260–280 compared to days 160–180. This is qualitatively as expected, since the cycle 23 solar maximum reached its peak in 2000–2002. The corresponding decrease in the strength of the interplanetary magnetic field allows an increasing flux of lower-energy GCR particles to reach the inner solar system. Larger increases are seen in subsequent years using the ULD, as will be described below, but the increase in this period is the first indication of the decline from the peak of cycle 23. This is consistent with the solar deceleration parameter  $\Phi$  values calculated in the Badhwar-O'Neill GCR model code. The code optionally uses CLIMAX neutron monitor data or ACE/CRIS data for input; the values quoted here used CLIMAX data. For days 160–180 of 2003, the code finds an average  $\Phi$  of 1443.5 MV, while the corresponding value for days 260–280 was 1181.1 MV. The model predicts that both A1 and A2 would have seen an increase of about 25% in the flux of protons and helium in this period, slightly more of an increase than is observed.

[56] In contrast to the other three channels, the flux in SCIH decreased by 5% over the period. This reflects a genuine decrease in the neutron flux reaching Odyssey from Mars. In quiet time, a large share of the SCIH counts are due to neutrons from Mars. That flux depends not only on the incident GCR flux (slowly varying during the 11 year solar cycle), but also on conditions in the atmosphere and on the surface (varying with Mars' 687 day orbit around the sun). As will become clearer in sections 5 and 6, when longer time periods are discussed, seasonal effects on Mars can outweigh the GCR modulation effects for purposes of the SCIH count rate. The trend seen in this time period is part of a seasonal cycle in which the high-

energy neutron flux falls and rises with CO<sub>2</sub> frost at the poles. The SCIH was normalized to MARIE data taken in 2002, centered on day 185, at which time the Martian solar longitude,  $L_s$ , was 36°; this was the tail end of northern spring, and Mars was approaching aphelion. The 5% decrease cited above occurred as  $L_s$  changed from about 206° (northern autumn) to 268° (northern winter), as Mars approached perihelion ( $L_s$  270°). At this time, CO<sub>2</sub> frost at the South Pole dissipates and reveals a permanent layer with a high content of water ice, which reduces the albedo flux of fast neutrons by moderating them to thermal energies. When CO<sub>2</sub> frost is present, this moderation is not seen, since the frost layer is sufficiently thick so as to obscure the effects of the water ice. One might naively expect this effect to be larger when the southern frost cap recedes, since it is larger and (as discovered fairly recently [Plaut et al., 2007]) the underlying layers have high water ice content, and indeed this is what the SCIH data seem to show.

#### 4.2.4. Days 299–303, 2003

[57] Figure 13 shows the fluxes measured from day 299, when the first indications of SPEs were seen, to day 302.3, when Odyssey entered safe mode. A short-lived spike is visible at 299.4 in both MARIE channels, and a gradual event of modest intensity began at 299.76. This event peaked at about day 300.25, with a particularly high A1/A2 SEP ratio close to 7. The SCIH SEP flux was higher than that seen in the ULD by about a factor of 2, consistent with previous observations during soft-spectrum events. The last uploaded MARIE data were at day 301.24. The instrument continued operating and was taking data when the large flux increase occurred at about 301.5. The failure caused the loss of this data, and the subsequent safe mode

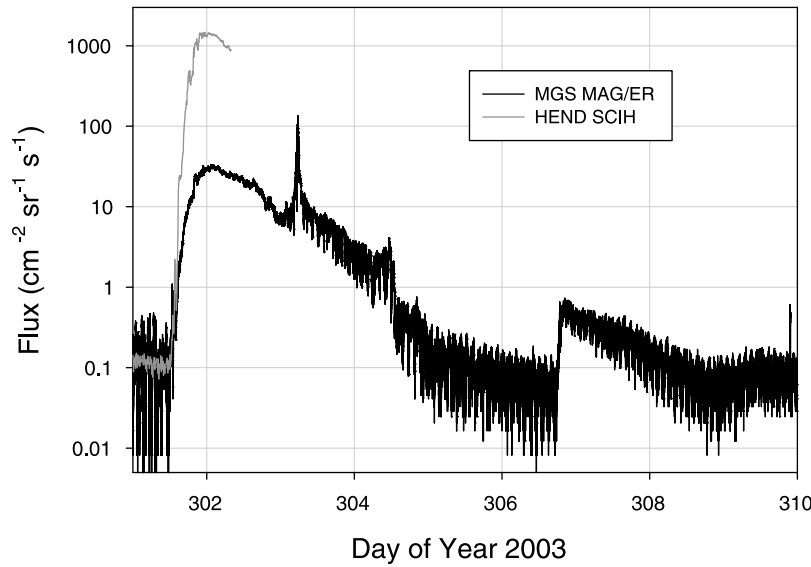


**Figure 14.** Data from the MGS Electron Reflectometer for the Halloween 2003 SPEs, also showing the last data collected by the HEND SCIH channel before the Odyssey safe-mode entry.

entry caused GRS and HEND to miss the remainder of the event as well. The ULD data for this event are unreliable past about 301.6, because the count rate became high enough to cause rollovers; the number of rollovers per measurement interval is not recorded.

[58] Since we have only partial data for the 28 October event, we focus first on the 26 October data. An unusual feature of this event is that it occurred when Earth and Mars were very nearly connected to the sun along exactly the same Parker spiral magnetic field line. ACE data show the solar wind speed averaged about  $470 \text{ km s}^{-1}$  from day 299.75 to day 301.0, so that perfect connection would occur for a longitudinal separation of about  $20^\circ$  in heliocentric coordinates; the actual separation on day 300 was about  $21^\circ$ . It is therefore of particular interest to compare the fluxes seen at Mars and near Earth. Archived GOES 11 data show integral proton fluxes for several channels, including channels I3, I4, and I5, with threshold energies  $E_{\text{proton}} > 10, 30, \text{ and } 50 \text{ MeV}$ . These can be taken to be in very approximate correspondence to the A1, A2, and ULD channels with 15, 27, and 42 MeV thresholds, respectively. The differences in threshold energies may be significant, especially in soft events when I3 would be expected to see a much higher flux than A1. We focus here on the event that began on day 299 (26 October) with a CME at 1754 (day 299.746). The A1 flux began to rise at about 299.76. The peak flux in the GOES data in I3, I4, and I5 is seen shortly after the start of the event, at 2235 (299.94). A gap in the MARIE data occurred between 299.85 and 300.08, so this peak may have been missed if it was dominated by the lower-energy protons that are seen in A1 but not the other Odyssey channels. There is a hint of a short-lived peak in the SCIH data around this time (299.93), but the SEP flux at that time was considerably smaller than at the

slightly later. The peak of the event as seen in all Odyssey channels was at 300.25; this may be due in part to the superposition of the orbit-related oscillations on top of the time-varying incident flux.

[59] Of perhaps more interest than the timing of the observations are the relative magnitudes of the fluxes. A conservative estimate of the radial gradient [Reames, 1999] predicts the flux ahead of the shock falls as  $R^{-3}$ , leading to a factor of 2.7 reduction at 1.4 AU. This is not close to what is observed; the peak A1 flux is on the order of 10 pfu, A2 about 2 pfu, SCIH and ULD both below 1 pfu. The GOES peaks were about 300, 40, and 10 pfu for I3, I4, and I5, respectively, in each case more than an order of magnitude higher than the roughly corresponding channels on Odyssey. Using a coupled transport-MHD heliospheric model, Kozarev *et al.* [2010] studied energetic particle transport of the Halloween events between 1 and 5 AU. They found that at energies of about 12 MeV and 54 MeV, peak fluxes decrease as  $R^{-3.49 \pm 0.31}$  and  $R^{-2.58 \pm 0.51}$ , respectively. Even a much steeper radial gradient (e.g.,  $R^{-4}$ ) cannot explain the observed differences.

[60] Although Odyssey went into safe mode, the remainder of this series of events was seen at Mars by the electron reflectometer instrument (ER) aboard the Mars Global Surveyor. The ER was primarily intended to measure low-energy electrons in several energy bins, probing the interaction of the solar wind with the Martian ionosphere. Heavier energetic charged particles also produce signals in the ER when they penetrate the instrument housing and hit the anode [Brain, 2006]. Figure 14 shows the ER data, along with SCIH data up until the Odyssey safing. The ER data are taken from the calibrated data products delivered to the PDS. The highest-energy electron channel (13–20 keV) is used with the default nor-

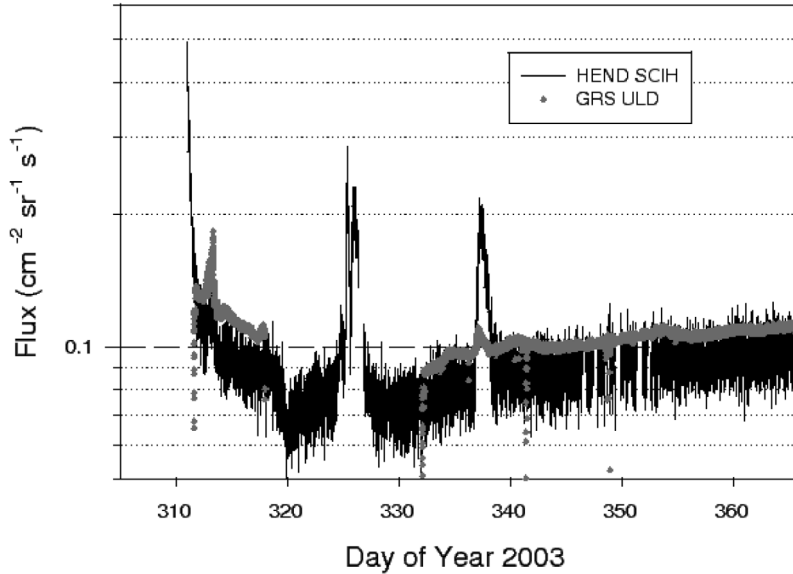


**Figure 15.** HEND and GRS data for the period after Odyssey recovered from safe mode to the end of 2003.

malization, which gives a quiet time differential flux of about  $0.1 \text{ cm}^{-2} \text{ sr}^{-1} \text{ s}^{-1} \text{ eV}^{-1}$ . This is numerically close to the integral fluxes seen in the MARIE and ULD channels, so as a matter of convenience we retain this normalization and treat the data as if they were integral fluxes. At the day 302 peak, the ER flux was about 30 pfu and the SCIH flux about 1400 pfu. Assuming isotropy, the event-integrated ER fluence from day 301 through 306 was  $1 \times 10^7 \text{ cm}^{-2}$ ; if the ratio of the peak fluxes holds for the event-integrated fluences, then the SCIH would have seen  $4.7 \times 10^8 \text{ cm}^{-2}$ , 3 orders of magnitude larger than in the July 2002 event.

### 5. Part III: Observations With GRS and HEND, November 2003 to May 2008

[61] After the loss of MARIE in October 2003, only the ULD and SCIH channels are available. Though neither has the sensitivity during SPE that MARIE had, they nonetheless provide a valuable record of fluctuations in the energetic particle environment in Mars orbit for the remainder of Odyssey's prime mission and two extended missions.

#### 5.1. November 2003 Through December 2004

[62] Figure 15 shows the SCIH and ULD fluxes for the remainder of 2003 after the main Halloween event. Odyssey recovered from safe mode and instruments were turned on starting on day 311. The GRS remained on until day 318, at which time an annealing cycle began. Normal GRS data acquisition resumed on day 332. When HEND data taking resumed, the SCIH was still seeing an above-normal flux which declined rapidly from 0.49 pfu at startup to the previous quiet time level within a day. A

short time later, near the end of day 312 (8 November), a small increase is seen in the ULD flux, which went from about 0.13 pfu to 0.18 pfu. This barely registered in the SCIH and is the only such occurrence observed in the entire data set.

[63] While the HPGe crystal was being annealed, SCIH recorded a Forbush decrease. The GCR flux reached a minimum of 0.065 pfu on day 320, less than half the quiet time level found in mid-2002. Another small SPE with a double-peak structure was seen in this period, lasting for about a day starting at 325.2. GCR levels returned to about 0.06 pfu subsequently. Finally, another small event is seen on day 337 in the SCIH and (barely) in the ULD. The GCR flux, which was rising slightly in the days prior to this event, continued to rise for the remainder of 2003 and for the first 180 days of 2004, as can be seen in Figure 16. (Note that this graph has a linear flux scale.) By day 179, the GCR flux reached 0.14 pfu and 0.13 in the ULD and SCIH, respectively.

[64] On day 180 of 2004, the SCIH count rate doubled, and remained at this level until day 187. This was the result of a test in which the normal triggering for the stilbene scintillator and its CsI anticoincidence shield was reversed. In normal operation, a neutron is defined by a stilbene hit with no anticoincidence hit. For this period, the trigger required a hit in the CsI, thus providing a direct measurement of charged particles. At 187.6, the trigger was switched back to its normal state, and just past 188.0, a very weak SPE began, shown in the inset graph in Figure 16. The ULD and SCIH recorded nearly identical peak fluxes, but since the SCIH quiet time flux was smaller than that measured by ULD, we can say that the SEP flux in SCIH was slightly larger than in ULD.

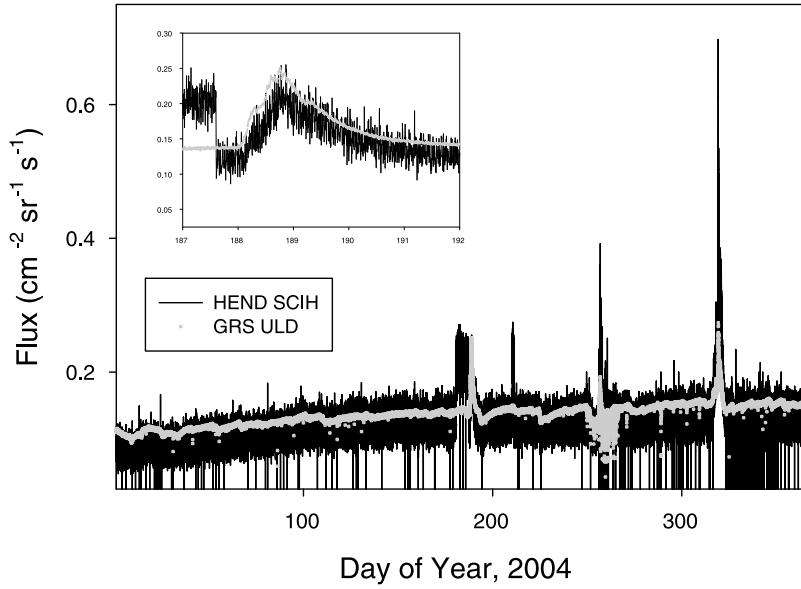


**Figure 16.** HEND and GRS flux data for 2004.

[65] Another test of the alternate SC trigger mode was run for 1 day starting at day 210.2, with the same result as the previous test (doubling of the count rate).

[66] Small SPEs are seen starting on days 256 and 316/317. In both, the ULD recorded peak fluxes only slightly higher than quiet time levels, while SCIH recorded somewhat higher (but still quite small) SEP fluxes.

## 5.2. January–February 2005

[67] Figure 17 shows the fluxes recorded in 2005. This plot shows a few interesting features: the GCR flux measured by the ULD rose throughout 2005; in contrast, the

SCIH shows a pronounced decrease in quiet time flux for at least 135 days starting at day 100; and three groups of SPEs are seen, one in January/February, one in July, and one in September. The outage in both channels from day 93 to day 97 was caused by a spacecraft safe-mode entry.

[68] Of particular interest is the January time period, when near-Earth detectors saw a series of significant SEPs. The GOES 11 I3, I4, and I5 proton channels recorded a series of increases starting on 15 January, with another on 16 January, and yet another on 17 January. Intensities remained relatively high and steady until 0700 on 20 January, when a large, impulsive event with a very hard

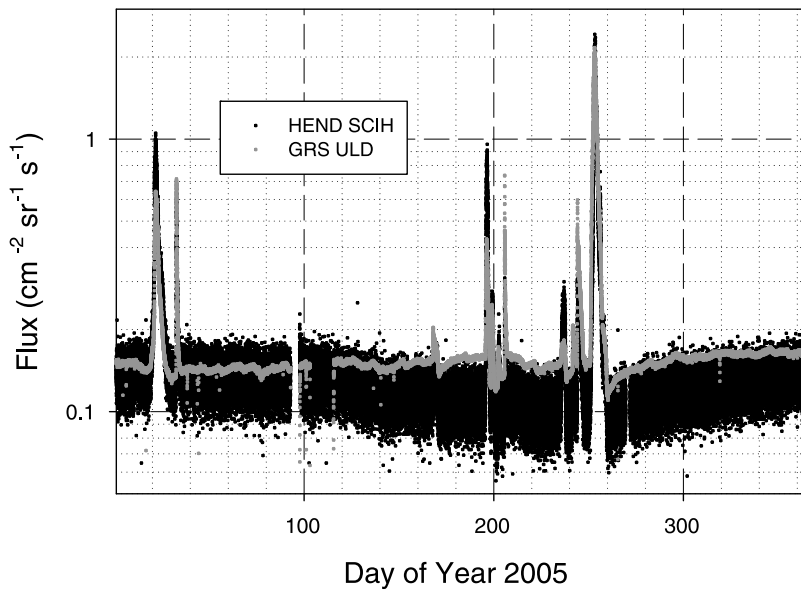


**Figure 17.** HEND and GRS flux data for 2005.

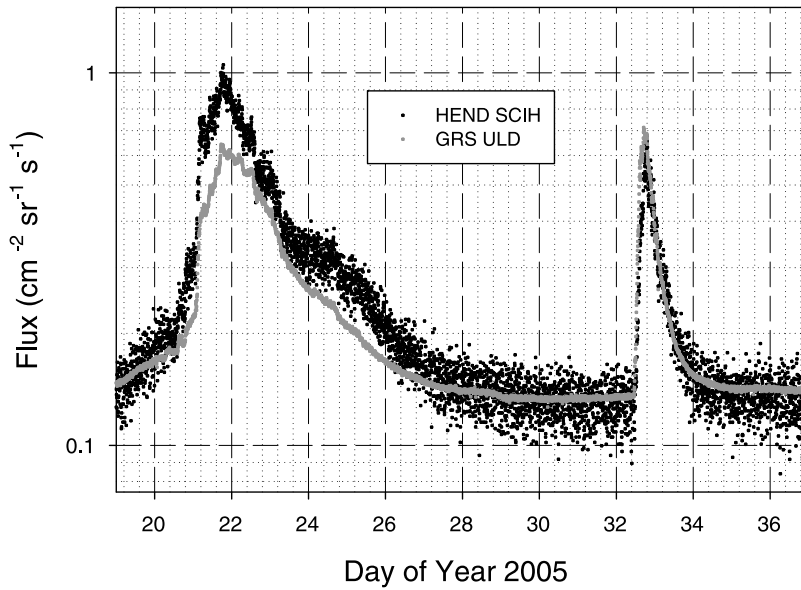


**Figure 18.** HEND and GRS data during the January–February solar activity in 2005.

spectrum occurred. The event was associated with a solar active region at  $15^{\circ}\text{N}$  latitude and  $5^{\circ}\text{W}$  longitude on the solar disk. Even in the GOES I7 channel (protons  $> 100$  MeV), the flux jumped by some 4 orders of magnitude. Fluxes remained high and did not return to quiet time levels until 23–24 January (depending on the energy threshold). In contrast, the SCIH and ULD saw no indication of solar activity until 20 January, when a weak event began. Peaks in both channels occurred on day 21, with SCIH at about 0.85 pfu and ULD at 0.45 pfu above quiet time levels. Mars at this time was leading Earth by about  $112^{\circ}$  of solar longitude, so any active regions on the sun that were well connected to Earth would have been poorly connected to Mars and vice versa. Intensities at Mars had returned to normal by day 28, 4–5 days later than at Earth, and on day 32.5 a small but rapid rise is seen in the ULD flux, shown in Figure 18. It is notable that the ULD count rate rose more rapidly than did the SCIH, and furthermore that the two channels peaked at different times, ULD at 32.7 and SCIH at 32.8. This indicates a hard-spectrum event. Maximum SEP fluxes were about 0.7 and 0.5 pfu for the two channels. The orbit-related oscillations can be seen in this event, particularly in SCIH. No solar activity is seen in the GOES proton data for this time.

[69] Although the rates seen near Earth and Mars are quite dissimilar in the late January/early February period, the ULD/SCIH comparison indicates a very weak but hard-spectrum event at Mars on day 32 reminiscent of that seen near Earth on day 20. Given the longitude difference between Earth and Mars, and the rapid rise of the ULD flux on day 32, this appears to have been a separate event and not a rotation of the aforementioned active region into magnetic connection with Mars.

[70] A small SPE was seen near Earth on days 167–168. A faint trace of the event can be seen in the Odyssey data, but the fluxes are only about 0.05 pfu above quiet time. At Mars, the Forbush decrease following this small event is actually more significant than the event itself, in that the suppression of the GCR below preevent levels lasted for some 14 days.

### 5.3. July 2005

[71] A series of four small SPEs is seen between days 195 and 208 (14–27 July), as shown in Figure 19. The quiet time fluxes in ULD and SCIH are somewhat different due to the Martian seasonal effect described above, with ULD averaging about 0.16 pfu and SCIH about 0.11 pfu. Both channels see a significant suppression of the GCR in the quiet periods between events. In the first three events, the peak SEP fluxes in SCIH are higher than in ULD (particularly in the first event), but in the fourth event ULD recorded a much larger peak SEP flux. In the first two events, peaking times are slightly earlier in the ULD. The longitudinal separation between Earth and Mars was about  $50^{\circ}$  during this period, with Mars leading. Small SPEs were also seen in GOES 11 on days 195 and 198, but no solar protons above 10 MeV were seen on day 202, nor on day 205.

### 5.4. August–September 2005

[72] The third and final series of SPEs seen at Mars in 2005 occurred between days 235 and 260 (23 August to 17 September). There were four events in the period, as shown in Figure 20. The first two were extremely minor, and may be correlated with weak events seen near Earth in the same time frame. Longitudinal separation between Earth and Mars was about  $30^{\circ}$ . GOES 11 data show an

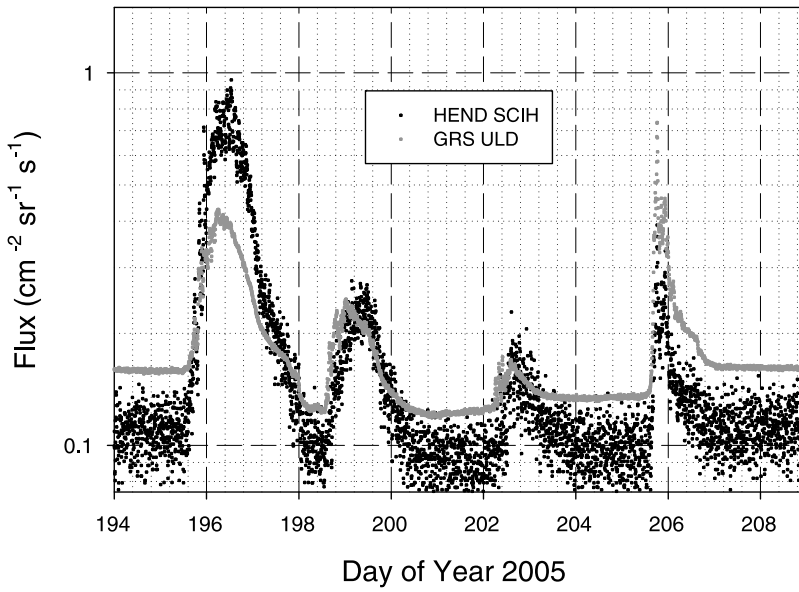


**Figure 19.** HEND and GRS data during the July 2005 solar activity.

increase in the I3 channel (protons above 10 MeV) early on 22 August (day 234) with a more pronounced increase later the same day, around 1900, accompanied by an increase in the I4 and I5 channels. The I4 and I5 increases persisted until day 236, while I3 remained elevated until day 238.

[73] In the third event, on day 244 (1 September), the ULD SEP flux exceeded that of the SCIHI, likely indicating a harder-than-normal spectrum. The largest of the four events began on day 251 (8 September) and produced

similar peaks in both channels, with ULD peaking earlier and SCIHI peaking very slightly higher. The ULD count rate rose faster than did the SCIHI rate. Elevated fluxes continued until day 259. A brief second burst of arriving SEPs is seen early on day 256. The fact that ULD and SCIHI fluxes are generally very close to one another throughout this later period suggests that this too was a comparatively hard-spectrum event. Near Earth on day 244, an extremely weak event was seen in the GOES 11 I2, I3, and I4 channels.

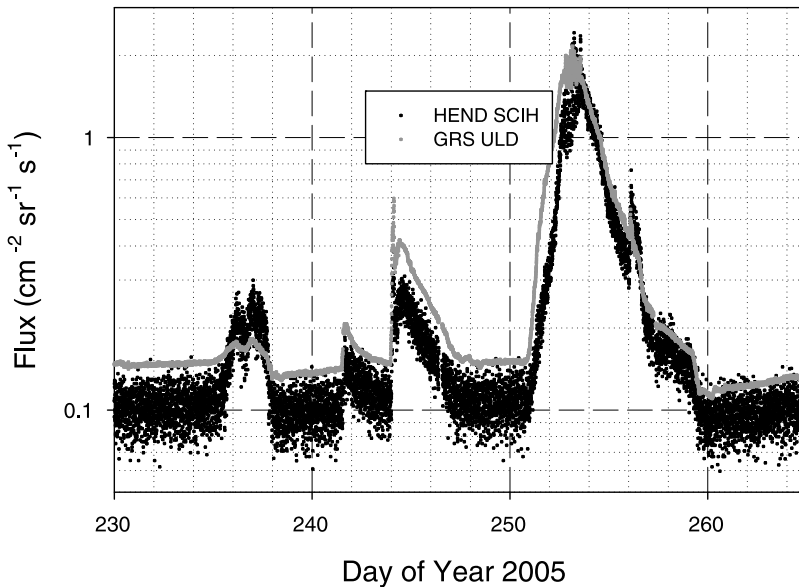


**Figure 20.** HEND and GRS data during the solar activity of August–September 2005.

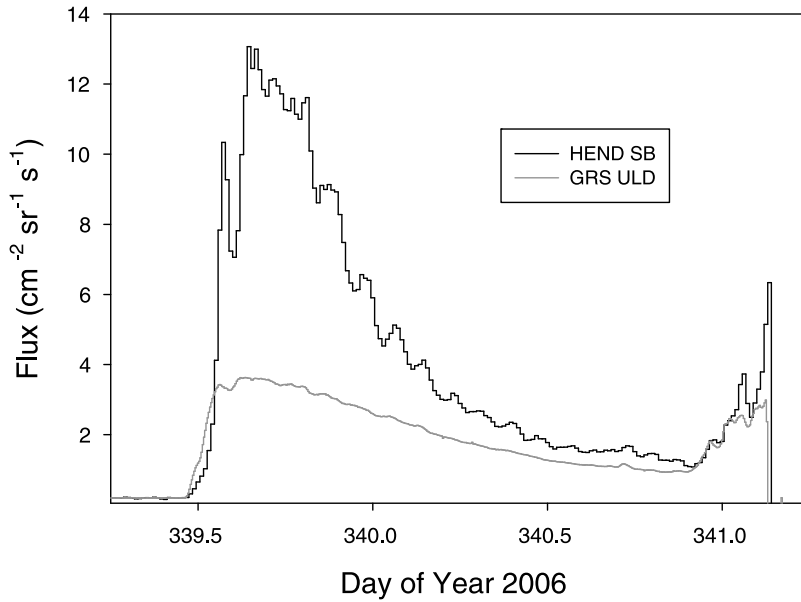


**Figure 21.** HEND and GRS data for the December 2006 solar activity.

### 5.5. January 2006 Through May 2008

[74] The solar activity seen both at Earth and at Mars in the second half of 2005 was nearly the last vestige of a very active solar maximum. From January through early December 2006, no SPEs were seen at Mars, and GCR levels as measured by the ULD and SCIH followed a generally upward trend, increasing from about 0.16 pfu to about 0.20 pfu just prior to the December event.

[75] In the 5 December (day 339.5) SPE, shown in Figure 21, the fluxes peak just a few hours after the onset of the event, with the SCIH flux reaching about 13 pfu and the ULD flux 3.3 pfu (with GCR backgrounds subtracted). Fluxes quickly fell, then rose again starting at 340.9. Odyssey underwent a safe-mode entry at 341.15, lasting until day 349.8. Mars led Earth by 157° of solar longitude at this time, so again we would not expect to observe the same event profiles in the two locations. In the GOES 11 I3 proton channel, a gradual SPE was seen to start on day 339, reaching its peak on day 341 and then slowly declining. The I4 and I5 channels returned to GCR levels by about day 347, but lower-energy channels remained elevated. An impulsive event was then seen starting at about 0300 UTC and peaking shortly thereafter. Odyssey had not yet recovered from safe mode when this second event began. However, when data taking resumed, count rates in both ULD and SCIH were at quiet time levels, whereas the GOES I4 and I5 channels were still slightly elevated.

[76] Following the solar activity in December 2006, both ULD and SCIH recorded a slight suppression in the GCR flux, which stayed relatively flat at about 0.2 pfu through early 2007. After a brief outage ending on day 19 of 2007, the ULD recorded an upward trend, a continuation of the

trend seen throughout most of 2006. However, over the first 160 or so days of 2007, the SCIH flux decreased. This is another instance of the seasonal effect described above. A time series with a longer baseline is shown below to clarify the point.

[77] The upward trend of the GCR flux through most of 2007 ceased for the first five months of 2008. The flux as measured by the ULD averaged 0.22 pfu, while the SCIH flux averaged 0.21 pfu. Both channels showed 5%–10% fluctuations around these averages, and the signals are for the most part highly correlated.

### 6. Long-Term GCR Modulation

[78] The available data span the period from February 2002 through the end of May 2008, more than half a solar cycle and encompasses most of an extraordinarily deep solar minimum. The weakening of the interplanetary magnetic field during solar minimum admits more GCR ions to the inner heliosphere than during times of greater solar activity. This is seen clearly at Mars as well as at Earth, as illustrated in Figure 22. These data are averaged over 3 h intervals for both channels. In addition to the rise of the GCR over time, other features of interest in Figure 22 are of interest, some of which were noted above. In particular, the seasonal variations of the SCIH count rate can be at least approximately correlated with  $L_s$  as indicated by the graph at the top of Figure 22. Dotted lines have been drawn corresponding to  $L_s = 270^\circ$ , which more or less coincides with the second and third SCIH local minima. It does not correspond to the first minimum, which is undoubtedly due to a combination of this seasonal effect and the strong Forbush decrease following the October 2003 SPEs. The second and third minima show drops of

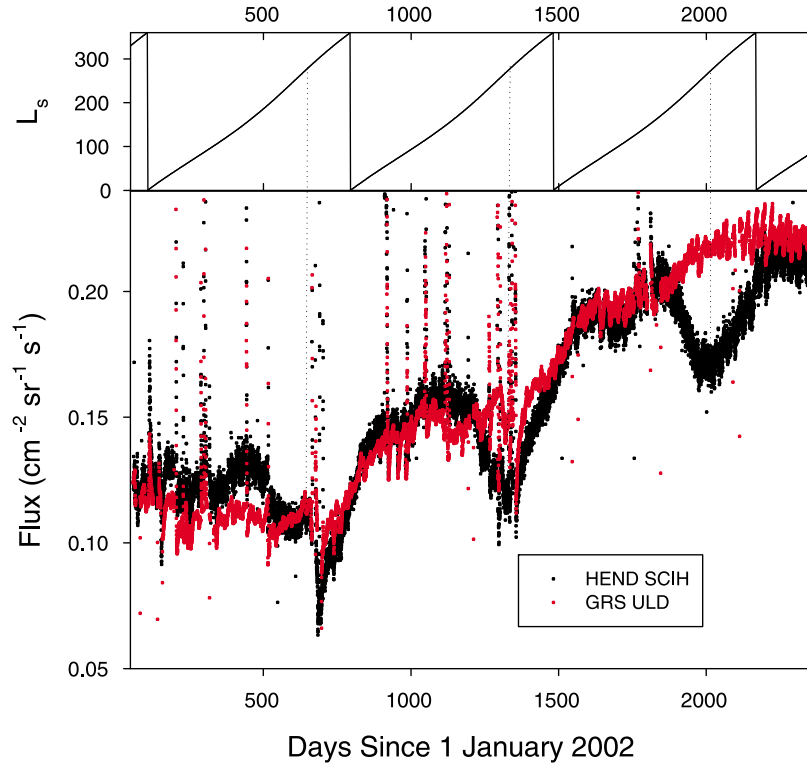


**Figure 22.** GCR fluxes in HEND and GRS from early 2002 to mid-2008, showing a factor of 2 rise in both channels, along with an additional seasonal effect seen in the SCIH neutron detector.

0.04–0.05 pfu with this normalization, or about 25% relative to the flux prior to the onset of the decreases; each of these minima occurs about 120 days after the start of the decrease.

[79] The seasonal effects are seen in the SCIH but not the GRS ULD, which provides a more satisfactory measurement of GCR modulation. We normalized the ULD data to mid-2002 quiet time, near the start of the Odyssey mission, and obtained a GCR flux of 0.115 pfu. By 2008, the average GCR flux had risen to about 0.22 pfu, with short-term peaks approaching 0.24 pfu, a doubling from mid-2002. From the standpoint of health risks to astronauts traveling to Mars or other deep-space destinations, the increase in the dose and dose equivalent from GCR may be more detrimental than the SPEs that occur closer to solar maximum, since in typical events the large majority of accelerated particles can be stopped by modest shielding.

[80] In late 2008, Odyssey performed a maneuver to change the orbit time from 0500 LMST/1700 LMST to 0345 LMST/1545 LMST in order to obtain a better signal-to-noise ratio in the thermal imaging system, THEMIS. This change effectively disables the GRS HPGe crystal, since the modified orientation places the sun in the field of view of the radiative cooler. Eight months after the propulsive maneuver, the spacecraft's drift to the earlier time was halted with a second maneuver. The GRS suite, which includes HEND, was off for most of the period between June and early November 2008. Additional data from

HEND will be available in the future. The effects of seasonal variations on apparent GCR flux that were shown above are on a timescale that is much shorter than the solar cycle, so that it should be possible to estimate the GCR flux even without the GRS ULD channel. Of greater importance for EMMREM and other SPE modeling efforts is the capability to continue to measure SEP fluxes as solar cycle 24 progresses toward its maximum. This will be possible as long as HEND continues to operate.

## 7. Comparison of MARIE Observations With EMMREM Predictions for May 2003 SEP Events

[81] Odyssey measurements, and particularly those from MARIE, provide a unique data set that allows us to estimate the radiation environment at Mars and improve our capability of predicting the arrival times of intense solar particle events in the vicinity of Mars. Figure 23 shows a comparison between MARIE differential proton intensities and those predicted by the Energetic Particle Radiation Environment Module (EPREM) during the May 2003 solar events at a similar median energy of 25 MeV. EPREM is a submodule of the Earth-Moon-Mars Radiation Environment Module [Schwadron *et al.*, 2010], which is a newly developed project aimed at characterizing the time-dependent radiation exposure in the interplanetary (IP) space and planetary environments. EPREM ingests SEP proton and heavy ion intensities measured at 1 AU

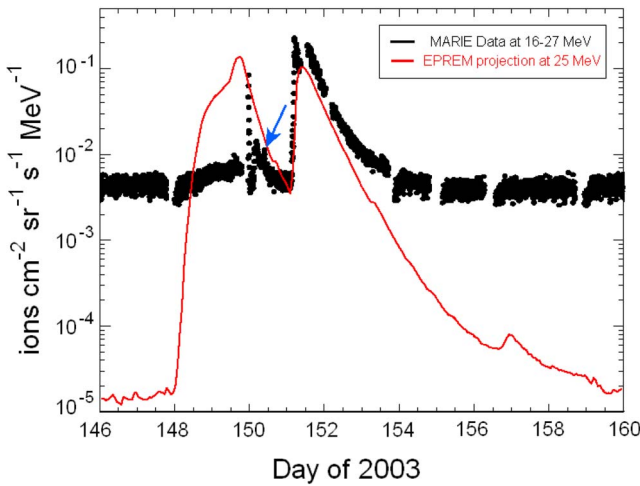


**Figure 23.** Proton intensities during the May 2003 SEP events as measured by MARIE at energies 16–27 MeV (black dots), along with the predicted proton intensities from the EMMREM/EPREM at 25 MeV (red trace). The blue arrow points to a possible interplanetary shock passage.

over a wide energy spectrum and projects them into the three-dimensional heliosphere. The code treats particles along each magnetic field line for transport, adiabatic focusing, adiabatic cooling, convection, pitch angle scattering, and stochastic acceleration in the framework of a modified formalism of the convection-diffusion-focused transport equation [Kota *et al.*, 2005]. It should be noted

that the difference in quiet time normalization between the data and the model seen in Figure 23 is an artifact. As described above, the quiet time A1 flux was always higher than that in A2, likely due to noise in A1 that is not accounted for in our normalization method.

[82] During the last week of May 2003, a series of CMEs lifted off from an active region (AR365) on the Sun and led to two major SEP events that were observed by multiple spacecraft near 1 AU. Particles from the first event arrived at Mars around day 148, followed by a second large enhancement that started on day 151.1 that was characterized by a fast rise and a slower decay phase. An IP-shock-associated energetic solar particle event (ESP) can also be identified during the first event, peaking at day 149.75. This ESP event had coincided with the arrival of two IP shocks at 1 AU.

[83] MARIE differential intensities are obtained by subtracting the A2 flux from the A1 flux, effectively creating a 16–27 MeV energy bin. The gap in the MARIE data shown for this same event in Figure 12 has been smoothed out by scaling from the ULD, which acquired data throughout the event. A closer inspection of the MARIE data in Figure 23 shows interesting features. A slight gradual enhancement above the background is observed during days 148–149.5, followed by a short-lived but high-intensity spike structure on day 150. Unfortunately, MARIE was downloading previously acquired data during the predicted onset of the first SEP event (day 148), it is thus impossible to ascertain whether there was any onset signature at Mars. Shortly after the spike, a decaying profile is observed between days 150.1 and 151. Within this decay, an abrupt increase that lasted for a short time

**Table 3.** Catalog of Solar Events Recorded by the Four Odyssey Detectors Studied Here, From 2002 to 2008<sup>a</sup>

Year	Start Day	Peak Day	End Day	Max. Flux In	Peak Flux (pfu)	Comments
2002	112	114	120	MARIE A1	0.4	Negligible SEP flux in other channels
2002	197	198	210	A1	90	MARIE off after day 198.7
2002	197	201	210	SCIH	84	Same event, second peak
2002	287	287	291	A1	3.2	
2002	298	298	300	A1	1.1	
2002	300	301	306	A1	59	
2003	77	78	79	A1	1.2	
2003	149	149	150	A1	1.0	Brief; not seen in other channels
2003	151	151	154	A1	3.1	Strong oscillations in A1
2003	299	300	301	A1	12	Last MARIE data
2003	301	301	unknown	SCIH	1470	Odyssey safe mode at day 302.3
2004	188	188	189	SCIH	0.1	SCIH mode switch just before rise
2004	256	256	257	SCIH	0.2	
2004	316	319	321	SCIH	0.3	
2005	19	21	25	SCIH	0.9	
2005	32	32	33	ULD	0.6	
2005	195	196	197	SCIH	0.8	
2005	198	199	199	SCIH	0.2	
2005	202	202	203	SCIH	0.1	
2005	205	205	206	ULD	0.6	
2005	235	237	237	SCIH	0.2	
2005	244	244	245	ULD	0.5	
2005	251	253	257	SCIH	2.3	
2006	339	339	unknown	SCIH	13	Event continued
2006	341	341	unknown	SCIH	6.1	Second peak; Odyssey safe mode at 341.1

<sup>a</sup>MARIE data were unavailable after October 2003.

can also be seen (marked by the blue arrow). The location of this structure (also see A1 trace in Figure 13) at day 151.15 is consistent with the arrival of an IP shock that was observed earlier at 1 AU, assuming that the shock maintained the same travel speed from 1 AU to Mars. In general, the intensity-time profile predicted by EPREM during the first SEP event is not seen in MARIE observations, which instead shows a more complex structure that appears to be related to this SEP event. However, it is not possible to estimate the peak flux or the fluence of this SEP event at Mars.

[84] The comparison of the EPREM prediction to the data for the second large SEP event is quite different than the first. As can be seen in Figure 23, the intensity-time profile predicted by EPREM for this event is in excellent agreement with MARIE observations. We note that during this period, the magnetic field line footprint connecting Mars to the solar surface was very close to the liftoff location of the CMEs associated with the second SEP event. More details on modeling this event at different locations in the heliosphere are given by *Dayeh et al.* [2010].

## 8. Conclusions

[85] Instruments aboard the Mars Odyssey spacecraft have been used to record the energetic charged particle environment in Mars orbit from 2002 to 2008. Weakening of the interplanetary magnetic field over this period of time leads to an observed doubling of the galactic cosmic ray flux. Defining a solar particle event as one in which a flux above concurrent GCR levels of at least 0.1 pfu was seen, 23 events (with 25 peaks) were recorded in this time, as cataloged in Table 3. The large majority of events were quite weak, with 12 of the 23 having peak SEP fluxes less than 1 pfu, and 7 others having peak SEP fluxes between 1 and 6.1 pfu. Peak SEP fluxes between 50 and 100 pfu were seen only twice (July 2002 and October 2002), and only in the large event of October 2003 was a flux above 1000 pfu recorded. (Two other events had peaks on the order of 10 pfu.) Of course, following the loss of MARIE in October 2003, the available HEND and GRS channels are insensitive to the lower-energy particles that MARIE (particularly the A1 counter) was able to detect, and this must be kept in mind when examining Table 3 and in summarizing the results.

[86] SPEs observed at Mars are not necessarily seen at Earth, and vice versa; in those instances where events were seen more or less simultaneously, fluxes were always much smaller at Mars. This can be due to narrow longitudinal distributions of the SEPs, and/or to scattering effects that cause the radial gradient to drop somewhat faster than  $R^{-3}$ . At the time of this writing, solar cycle 24 had just begun. As the cycle progresses, it will be useful to continue to monitor SPEs using HEND's SCIH channel, applying due caution to the interpretation of the data since this channel is sensitive to seasonal effects on Mars.

[87] The large majority of the data presented here are simply time series of the flux as seen in various counters.

These are contained in a small number of files (one per calendar year) and are available from the lead author on request. Alternatively, since all the data are in the PDS archives, anyone choosing to do so can perform a similar analysis.

## Appendix A: MARIE Hardware Issues

[88] The MARIE detectors, preamplifiers, and shaping amplifiers worked as expected. The bulk of the problems were with the digital electronics, which suffered from several design and performance problems. The issues can be roughly grouped into three categories: dynamic range, rate, and efficiency. There were data gaps for various reasons; these are also described in the following.

### A1. Dynamic Range

[89] The dynamic range of the MARIE pulse height readout was small compared to the range of energy deposition encountered in the deep space environment, therefore only some charged particles can be identified. The gains of the A and B detectors were set so that the maximum  $dE/dx$  in silicon was about 60 MeV/mm; higher values of  $dE/dx$  caused saturation in the electronics. In radiation biology, the quantity LET (linear energy transfer) in water is used rather than  $dE/dx$  in silicon, but for sufficiently energetic particles the two are approximately related by a constant, which is about 1.8. The average path length of a particle in the viewing cone is about 10% greater than that of a particle at normal incidence, so that on average LETs up to about 30 keV/ $\mu\text{m}$  can be measured. For highly relativistic particles, at or near the minimum of the  $dE/dx$  versus energy curve, this corresponds to about charge 12 (Mg). This is an unfortunate limitation since the radiation dose and dose equivalent in free space are strongly weighted by particles heavier than Mg, in particular silicon (charge 14) and iron (charge 26). These ions, and all other particles heavier than Mg, were registered as hits in MARIE, but with no useful pulse height information due to saturation. A small subset of these events produced usable hits in the Cerenkov detector, and some very low resolution particle identification is possible in those cases.

[90] Energy depositions from helium ions ( ${}^4\text{He}$ ) below about 200 MeV/nucleon were in the "sweet spot" of the dynamic range, allowing for determination of the energy. High-energy He ions can also be easily identified, but with no directional information. The differential flux of He below 150 MeV/nuc was measured and is published elsewhere [Lee, 2006].

### A2. Pulse Height Readout Rate

[91] As mentioned in the main body of the text, MARIE pulse height data were corrupted if an event triggered within about 400 ms of the previous event. Given a total GCR flux of about  $0.2 \text{ cm}^{-2} \text{ sr}^{-1} \text{ s}^{-1}$  and the telescope's geometric factor of  $5.62 \text{ cm}^2 \text{ sr}$  for highly penetrating particles, the expected GCR rate was 1.1 Hz. Running with

the trigger set to fire on all GCR protons would have yielded a data set with about 35% of events corrupted during solar quiet time. This was noticed during the cruise to Mars, and thresholds were raised on the A1 and A2 discriminators so that high-energy protons did not fire the coincidence trigger. This reduced the share of corrupted events to a little over 20%, but meant that the high-energy proton flux was for the most part not measured. The threshold was adjusted slightly downward during the orbital phase of the mission.

[92] Corrupted events can be eliminated from the analyzed sample by requiring a minimum time separation of 400 ms between events. This necessitates a live time correction of 1.27, even during solar quiet time. The live time decreases significantly as the rate increases. In retrospect, a better strategy would have been to keep the trigger threshold low and accept the higher share of corrupted events (which could have been discarded in the analysis).

### A3. Cerenkov and PSD Performance

[93] The Cerenkov ("C") detector was intended to measure particle velocities below about 450 MeV/nucleon, and to provide directional discrimination (only particles entering MARIE from the front can produce detectable Cerenkov light). Even particles above the saturation level would produce a signal, so there should at least be an indication of direction. However, the Cerenkov detector suffered from very low efficiency due to insufficient voltage on the photomultiplier tube, and those data are not used here. There is therefore no directional discrimination in the MARIE data, except for those events in which relatively low energy particles either stopped in the detector stack or had a significant increase in their dE/dx as they traversed the stack.

[94] Each channel in the strip detectors was read separately, and an algorithm implemented in hardware to find hits. This was needed for zero suppression. However, amplifier gains on these channels were set high and thresholds low, so that on any given event many strips appeared to be hit. The hit-finding algorithm was not sufficiently robust under these conditions, rendering the PSD data unusable.

### A4. Data Gaps

[95] Many gaps in the MARIE data were a by-product of the commanding sequence, in which data uploads to the spacecraft were not immediately followed by commands to restart acquisition. The restart commands were sent in a subsequent communication session, which did not necessarily occur soon after the upload. This was resolved later in the mission. MARIE outages were also caused when its storage area was nearly full; acquisition was halted until data could be uploaded. This was a particular problem during SPEs, when the disk filled at faster-than-normal rates.

### A5. Backward Going Ions in MARIE

[96] For particles entering MARIE from the front (striking A1 first), the geometric factor for the coincidence trigger is

$3.19 \text{ cm}^2 \text{ sr}$ , assuming an isotropic incident distribution. MARIE sits on Odyssey's equipment deck and has an unobstructed field of view in the forward direction but is shielded by various objects, including the decks, in the rear. Particles entering the detector in the forward direction encounter only the spacecraft's very thin thermal blanket (0.13 mm of mylar) and the thin aluminum case (1.27 mm) that contains the MARIE hardware. This light shielding in the forward direction determines the lower limit of 16 MeV of energy for a proton to reach A1. An additional 11 MeV of kinetic energy is required to penetrate the PSDs and reach A2, making that threshold 27 MeV.

[97] Backward going ions are defined as those entering MARIE from the end opposite A1. One can draw a cone corresponding to the field of view defined by the A1 and A2 detectors; about 45% of the solid angle in this cone is occluded by Mars, and most of the unshadowed portion is shielded by various components of the spacecraft. The geometry factor for the portion of the field of view not shadowed by Mars has been calculated to be  $2.43 \text{ cm}^2 \text{ sr}$ , using the Monte Carlo method described by Sullivan [1971].

[98] Directly behind MARIE is the propulsion module core, which includes two fuel tanks. On launch, the tanks were filled with  $\text{N}_2\text{O}_4$  fuel that was completely used in Mars Orbit Insertion. The titanium shell is thin; the wall has an areal density of about  $1 \text{ g cm}^{-2}$  and does little to shield the rear field of view. Of greater importance for shielding are the electronics boxes deployed on the equipment deck. These include two Small Deep Space Transponders and the Command and Data Handler (C&DH). A particle on a trajectory to enter MARIE from the backward direction, through the C&DH, traverses, on average, about  $13 \text{ g cm}^{-2}$  of shielding. Before reaching A2, the particle sees another  $2 \text{ g cm}^{-2}$  of shielding from the shell of the oxidizer tank,  $5 \text{ g cm}^{-2}$  from the Schott glass in MARIE, and another  $5 \text{ g cm}^{-2}$  from the MARIE B detectors, for a total of  $25 \text{ g cm}^{-2}$ . Some of the backward going trajectories that reach A2 and A1 traverse the C&DH and other materials, but miss the Schott glass, since it is smaller in area than the A detectors.

[99] Such large depths of shielding greatly affect the flux of particles that reach MARIE from the backward direction. Two physical effects are important as energetic particles traverse matter: ionization energy loss and nuclear interactions. The former effect causes particles to slow down and, if the energy is low enough, to stop; the latter causes fragmentation of the incident heavy ions into lighter fragments. A depth of  $25 \text{ g cm}^{-2}$  of aluminum will stop iron ions below 800 MeV/nuc, silicon ions below 550 MeV/nuc, carbon ions below 350 MeV/nuc, and protons below 170 MeV. For purposes of nuclear fragmentation, a carbon ion traversing aluminum has a mean free path of about  $45 \text{ g cm}^{-2}$ , so we expect that only 57% of the incident ions would survive to reach A2; the corresponding percentages for incident Si and Fe ions are 42% and 33%, respectively.

**Table A1.** Trigger Rates for Cosmic Ray Muons at Sea Level Using the MARIE Flight Spare Unit

Threshold Setting	Events per Day	Fraction of Expected Rate
819	926.3	0.269
81B	919.2	0.267
81E	563.6	0.164
81E <sup>a</sup>	702.9	0.204
82D <sup>a</sup>	792.0	0.230

<sup>a</sup>These tests were performed with a revised flight software package.

## A6. Trigger Threshold Studies

[100] As described above, during Odyssey's cruise to Mars, the MARIE threshold was raised to (partially) eliminate events with corrupted pulse height records. The threshold was subsequently lowered during the orbital phase, but was still far higher than optimal. Two tests were undertaken using flight spare hardware, aimed at estimating the trigger efficiency as a function of the flight parameters. As we will explain, the tests were inconclusive, but tend to point to a trigger efficiency on the order of 20% for minimum-ionizing particles.

[101] In the first test, the full MARIE flight spare unit was oriented with the telescope pointing upward to detect cosmic ray muons. Lengthy runs (several days) were taken with various threshold settings. Data were collected and analyzed to determine the recorded event rate, which was compared to the known flux of sea level muons. Results are shown in Table A1. The hexadecimal numbers used to control the threshold settings have no intrinsic meaning; these values were uploaded to set the output level of a digital-to-analog converter (DAC) that provides for each channel a DC input to a comparator. An increasing value corresponds to an increase in the trigger threshold. The second input to the comparator came from the fast amplifier that is part of the analog signal chain. The results shown in Table A1 are difficult to understand. The first three results are sensible: settings of 819, 81B, and 81E yield decreasing rates, as expected. However, a second test at 81E yielded a higher rate than the first test, and a test at the value used in flight, 82D, yielded an even higher efficiency. The latter two tests were performed using a different version of the flight software which did not correspond to the software actually running on the flight unit.

[102] The second test was performed using only two circuit boards of the type used for the A detectors and the CPU board. In this test, the onboard calibration circuit (not used in flight) was used to inject known values of charge into the preamplifiers. The pulse injection ran at a fixed rate of 4.12 Hz. Pulse amplitudes and trigger thresholds were both varied. The results are shown in Table A2. They indicate that at the 82D threshold setting used for the acquisition of most of the flight data, there was virtually no trigger efficiency for energy depositions below 1 MeV. A high-energy GCR proton deposits an average of 0.33 MeV in a 1 mm silicon detector at normal incidence, far below this threshold.

[103] The test results are inconsistent. The cosmic ray muon tests are more consistent with the flight data, in which there is evidently some efficiency even for minimum-ionizing particles. The pulse injection test would lead us to conclude that there was essentially no efficiency for protons with energies above about 200 MeV, which is clearly not the case. On the other hand, even with the somewhat more pessimistic results obtained with charge injection, we would conclude that MARIE triggered with high efficiency on high-energy helium ions, which deposit an average of 1.33 MeV in a 1 mm silicon detector for particles at normal incidence. (Energy deposition increases as the angle of incidence increases so normal incidence is the worst case.)

## Appendix B: Readout and Processing of GRS and HEND Data

[104] The GRS and HEND data are read out at intervals of approximately 19.76 s. Readout of the Ge crystal includes the full energy spectrum recorded in the interval, as well as the count of hits that fire the ULD. Pulses from each HEND sensor are digitized in four bits (16 channels) and those spectra are recorded in the same time intervals, synchronized with the GRS's readout. Data are downloaded from Odyssey to Earth at least once a day, and undergo considerable processing before being archived in the PDS.

[105] All data used in the present analysis are in the PDS, where they are categorized by the level of processing. The GRS data used here were downloaded from the PDS as binary raw data (EDR), for which one "gamma spectrum" file is provided per day. All such files are filtered to obtain, for each 19.76 s interval, the precise time in the middle of the interval and the count of hits in the ULD. These two pieces of information are extracted from each record and saved in a file format readable by the data analysis package PAW [Brun *et al.*, 1989].

[106] The HEND data used here are from the most recent PDS releases as of 2009. (A bug fix and implementation of a solar modulation correction have led to revisions of the

**Table A2.** Results From Pulse Injection Tests at the "82D" Threshold Setting

Injected $\Delta E$ Equivalent (MeV)	Trigger Efficiency
0.9426	0.0016
0.9730	0.0073
1.0034	0.0355
1.0338	0.0557
1.0642	0.0719
1.0946	0.1099
1.1250	0.1809
1.1554	0.2835
1.1858	0.3578
1.2162	0.5089
1.2466	0.6535
1.2770	0.8368
1.3074	0.9661
1.3378	0.9976
1.3682	1.0000

data products over time.) The raw, uncorrected counts for all HEND detectors are extracted from the binary data and saved in a PAW-readable file, along with the available value of the Mars solar longitude,  $L_s$ . Because the rates are low, 15 min time intervals are used for HEND data to obtain reasonable counting statistics, compared to the 5 min binning used for MARIE and GRS data.

[107] **Acknowledgments.** We express our profound thanks to the many people who supported this effort over many years, both on the individual instrument teams for MARIE, GRS, and HEND, and on the 2001 Mars Odyssey project. Odyssey has had a remarkably long and successful mission thanks in large part to the management team, which over the years has included Robert Gibbs, Robert Mase, Gaylon McSmith, Phillip Varghese, Steve Saunders, Jeffrey Plaut, and David Senske. And of course this work would not have been possible without the tireless efforts of the original MARIE Principal Investigator, the late Gautam Badhwar. He is greatly missed. This work was supported at LBNL by NASA grant NNN05AA471 and at Southwest Research Institute by NASA grant NNX07AC12G.

## References

- Andersen, V., L. Pinsky, K. Lee, C. Zeitlin, T. Cleghorn, F. A. Cucinotta, P. B. Saganti, W. Atwell, and R. Turner (2003), Monte Carlo simulation of the response of MARIE, in *28th International Cosmic Ray Conference*, edited by T. Kajita et al., pp. 2113–2116, Universal Acad., Tokyo.
- Badhwar, G. D. (2004), Martian Radiation Environment Experiment (MARIE), *Space Sci. Rev.*, **110**, 131–142, doi:10.1023/B:SPAC.0000021009.68228.a8.
- Badhwar, G. D., and P. M. O'Neill (1992), An improved model of galactic cosmic radiation for space exploration missions, *Nucl. Tracks Radiat. Meas.*, **20**, 403–410, doi:10.1016/1359-0189(92)90024-P.
- Boynton, W. V., et al. (2002), Distribution of hydrogen in the near surface of Mars: Evidence for subsurface ice deposits, *Science*, **297**, 81–85, doi:10.1126/science.1073722.
- Boynton, W. V., et al. (2004), The Mars Odyssey Gamma-Ray Spectrometer instrument suite, *Space Sci. Rev.*, **110**, 37–83, doi:10.1023/B:SPAC.0000021007.76126.15.
- Brain, D. A. (2006), Mars Global Surveyor measurements of the Martian solar wind interaction, *Space Sci. Rev.*, **126**, 77–112, doi:10.1007/s11214-006-9122-x.
- Brun, R., O. Couet, C. E. Vandoni, and P. Zanarini (1989), PAW, a general-purpose portable software tool for data analysis and presentation, *Comput. Phys. Commun.*, **57**, 432–437, doi:10.1016/0010-4655(89)90257-9.
- Committee on the Evaluation of Radiation Shielding for Space Exploration, National Research Council (2008), *Managing Space Radiation Risk in the New Era of Space Exploration*, Natl. Acad. Press, Washington, D. C.
- Dayeh, M. A., M. I. Desai, K. Kozarev, N. A. Schwadron, L. W. Townsend, M. PourArsalan, C. Zeitlin, and R. B. Hatcher (2010), Modeling proton intensity gradients and radiation dose equivalents in the inner heliosphere using EMMREM: May 2003 solar events, *Space Weather*, doi:10.1029/2009SW000566, in press.
- Ellison, D. C., and R. Ramaty (1985), Shock acceleration of electrons and ions in solar flares, *Astrophys. J.*, **298**, 400–408, doi:10.1086/163623.
- George, J. S., et al. (2009), Elemental composition and energy spectra of galactic cosmic rays during solar cycle 23, *Astrophys. J.*, **698**, 1666–1681, doi:10.1088/0004-637X/698/2/1666.
- Hurley, K., et al. (2006), Mars Odyssey joins the third interplanetary network, *Astrophys. J. Suppl. Ser.*, **164**, 124–129, doi:10.1086/501352.
- Kota, J., W. B. Manchester, and T. I. Gombosi (2005), SEP acceleration at realistic CMEs: Two sites of acceleration?, in *29th International Cosmic Ray Conference*, vol. 1, edited by B. Sripathi Acharya et al., pp. 125–128, Tate Inst. of Fundam. Res., Mumbai, India.
- Kozarev, K., N. A. Schwadron, M. A. Dayeh, L. W. Townsend, M. I. Desai, and M. PourArsalan (2010), Modeling the 2003 Halloween events with EMMREM: Energetic particles, radial gradients, and coupling to MHD, *Space Weather*, doi:10.1029/2009SW000550, in press.
- Lee, K. T. (2006), Martian Radiation Environment Experiment (MARIE), Ph.D. dissertation, Univ. of Houston, Houston, Tex.
- Lingenfelter, R. E., E. H. Canfield, and W. N. Hess (1961), The lunar neutron flux, *J. Geophys. Res.*, **66**, 2665–2671, doi:10.1029/JZ066i009p02665.
- Luhmann, J. G., C. Zeitlin, R. Turner, D. A. Brain, G. Delory, J. G. Lyon, and W. Boynton (2007), Solar energetic particles in near-Mars space, *J. Geophys. Res.*, **112**, E10001, doi:10.1029/2006JE002886.
- Moyers, M. F., P. B. Saganti, and G. Nelson (2006), EVA space suit proton and electron threshold energy measurements by XCT and range shifting, *Radiat. Meas.*, **41**, 1216–1226, doi:10.1016/j.radmeas.2006.04.033.
- Plaut, J. J., et al. (2007), Subsurface radar sounding of the south polar layered deposits of Mars, *Science*, **316**, 92–95, doi:10.1126/science.1139672.
- Reames, D. (1999), Solar energetic particles: Is there time to hide?, *Radiat. Meas.*, **30**, 297–308, doi:10.1016/S1350-4487(99)00066-9.
- Saunders, R. S., et al. (2004), 2001 Mars Odyssey mission summary, *Space Sci. Rev.*, **110**, 1–36, doi:10.1023/B:SPAC.0000021006.84299.18.
- Schwadron, N. A., et al. (2010), Earth-Moon-Mars Radiation Environment Module framework, *Space Weather*, **8**, S00E02, doi:10.1029/2009SW000523.
- Shikaze, Y., et al. (2007), Measurements of 0.2–20 GeV/n cosmic-ray proton and helium spectra from 1997 through 2002 with the BESS spectrometer, *Astropart. Phys.*, **28**, 154–167, doi:10.1016/j.astropartphys.2007.05.001.
- Sullivan, J. D. (1971), Geometric factor and directional response of single and multi-element particle telescopes, *Nucl. Instrum. Methods*, **95**, 5–11, doi:10.1016/0029-554X(71)90033-4.
- Townsend, L. W., J. W. Wilson, J. L. Shinn, and S. B. Curtis (1992), Human exposure to large solar particle events in space, *Adv. Space Res.*, **12**, 339–348, doi:10.1016/0273-1177(92)90126-I.
- Tylka, A. J., and W. F. Dietrich (1999), IMP-8 observations of the spectra, composition, and variability of solar heavy ions at high energies relevant to manned space missions, *Radiat. Meas.*, **30**, 345–359, doi:10.1016/S1350-4487(99)00062-1.
- Vazquez, M. E. (1998), Neurobiological problems in long-term deep space flights, *Adv. Space Res.*, **22**, 171–183, doi:10.1016/S0273-1177(98)80009-4.
- Zeitlin, C., T. Cleghorn, F. A. Cucinotta, P. B. Saganti, V. Andersen, K. Lee, L. Pinsky, W. Atwell, R. Turner, and G. D. Badhwar (2004), Overview of the Martian Radiation Environment Experiment, *Adv. Space Res.*, **33**, 2204–2210, doi:10.1016/S0273-1177(03)00514-3.
- W. Atwell, Boeing Company, 1600 Smith St., Houston, TX 77002, USA. (william.atwell@boeing.com)
- W. Boynton, Lunar and Planetary Laboratory, University of Arizona, Tucson, AZ 85721, USA. (wboynton@pl.arizona.edu)
- T. F. Cleghorn, F. A. Cucinotta, and K. T. Lee, NASA Johnson Space Center, 1601 NASA Pkwy., Houston, TX 77058, USA. (timothy.f.cleghorn@nasa.gov; francis.a.cucinotta@nasa.gov; kerry.t.lee@nasa.gov)
- M. Dayeh and M. Desai, Southwest Research Institute, 6220 Culebra Rd., San Antonio, TX 78238, USA. (maldayeh@swri.edu; mdesai@swri.edu)
- S. B. Guedersloh, Department of Nuclear Engineering, Texas A&M University, 3133 TAMU, College Station, TX 77843, USA. (guedersloh@tamu.edu)
- D. Hassler and C. Zeitlin, Southwest Research Institute, 1050 Walnut St., Ste. 300, Boulder, CO 80302, USA. (hassler@boulder.swri.edu; zeitlin@boulder.swri.edu)
- K. Kozarev and N. A. Schwadron, Department of Astronomy, Boston University, 725 Commonwealth Ave., Boston, MA 02215, USA. (kamen@bu.edu; nathanas@bu.edu)
- I. Mitrofanov, Space Research Institute, 84/32 Profsoyuznaya Str., Moscow 117997, Russia. (mitrofanov@l503.iki.rssi.ru)
- L. Pinsky, Physics Department, University of Houston, Houston, TX 77204, USA. (pinsky@uh.edu)
- P. Saganti, Department of Physics, Prairie View A&M University, Prairie View, TX 77446, USA. (pbsaganti@pvam.edu)
- R. Turner, Analytic Services Inc., 2900 South Quincy St., Ste. 800, Arlington, VA 22206, USA. (ron.turner@anser.org)